DEVELOPMENT OF A PROMPT-GAMMA, NEUTRON-ACTIVATION ANALYSIS FACILITY AT THE TEXAS A&M UNIVERSITY NUCLEAR SCIENCE CENTER

A Thesis

by

OTU EFFIONG INYANG

Submitted to the Office of Graduate Studies of
Texas A&M University
in partial fulfillment of the requirements for the degree of

MASTER OF SCIENCE

August 2008

Major Subject: Health Physics

DEVELOPMENT OF A PROMPT-GAMMA, NEUTRON-ACTIVATION ANALYSIS FACILITY AT THE TEXAS A&M UNIVERSITY NUCLEAR SCIENCE CENTER

A Thesis

by

OTU EFFIONG INYANG

Submitted to the Office of Graduate Studies of
Texas A&M University
in partial fulfillment of the requirements for the degree of

MASTER OF SCIENCE

Approved by:

Chair of Committee,	W. Daniel Reece
Committee Members,	John W. Poston, Sr.
	Michael A. Walker
Head of Department,	Raymond J. Juzaitis

August 2008

Major Subject: Health Physics

ABSTRACT

Development of a Prompt-Gamma, Neutron-Activation Analysis Facility at the Texas A&M University Nuclear Science Center. (August 2008)

Otu Effiong Inyang, B.Sc., University of Calabar, Nigeria

Chair of Advisory Committee: Dr. W. Daniel Reece

A prompt-gamma, neutron-activation analysis facility earlier developed at the Nuclear Science Center of Texas A&M University could not be used successfully to analyze geologic samples due to high detection background, low neutron fluence rate and poor detection equipment . A systematic investigation into the performance capability of a prompt-gamma, neutron activation analysis facility was undertaken in this research project. The facility was reconstructed and used to obtain prompt-gamma spectra of chlorine and cadmium and from the spectra, the net peak area counts for the most intense prompt-gamma-ray energies were obtained. A theoretical model was developed which can predict the net peak area counts expected on these prompt-gamma-ray energies using the thermal neutron fluence rate at the sample position, the absolute efficiency of the detector, and the mass and partial gamma-ray production cross section data for the samples. The experimental and predicted results were compared to establish the performance capability of the reconstructed facility. Good agreements between experimental and predicted results were obtained for chlorine, but results from cadmium showed larger discrepancies due to self-shielding effects. Corrections for self-shielding

effects were applied to results from cadmium and the experimental and predicted results were also in good agreement. The satisfactory results indicate that it is possible to implement the prompt-gamma, neutron-activation analysis technique at Beam Port #1 of the Nuclear Science Center Reactor. To be able to obtain excellent results from other samples, improvements in shielding materials to attain a lower detection background and a highly efficient detection system should be incorporated.

DEDICATION

To my wife, Rosemary for her support, love and encouragement

To our children, Mfon and Chidera for their patience

To my parents

And to God Almighty for His mercies

ACKNOWLEDGEMENTS

I would like to thank my committee chair, Dr. W. Daniel Reece, and my committee members, Dr. John Poston Sr. and Dr. Michael Walker, for their guidance and support throughout the course of this research.

The members of the faculty and staff of the Texas A&M Nuclear Engineering Department were very generous in their support and I remain grateful. Thanks also go to my friends and colleagues for making my time at Texas A&M University a great experience. Especially, I want to thank Dr. Latha Vasudevan who not only initiated this project, but provided invaluable assistance and advice during the course of this work. My thanks also go to Dr. Dennis James and Mr. Rick Harrison who provided valuable suggestions and guidance on the Prompt-Gamma, Neutron-Activation Analysis studies. My appreciation would be incomplete without mentioning the numerous contributions of the staff of the Nuclear Science Center, most of whom assisted with the construction and testing of this facility.

Funding for the instrumentation on this research was provided by the DOE Reactor Instrumentation Grant DE-PS07-061D-14718.

NOMENCLATURE

PGNAA	Prompt-Gamma, Neutron-Activation Analysis
NAA	Neutron-Activation Analysis
PGAA	Prompt-Gamma Activation Analysis
INAA	Instrumental (or Conventional) Neutron-Activation Analysis
NSC	Nuclear Science Center, Texas A&M University

TABLE OF CONTENTS

CHAPTER Page

LIST OF FIGURES

FIGURE Page

LIST OF TABLES

CHAPTER I

INTRODUCTION

Neutron-activation analysis (NAA) is used as an analytical technique to determine elemental concentrations in a wide variety of samples. The technique is based on the radiative capture of neutrons, one of the most fundamental nuclear reactions. Upon neutron capture, the resulting compound nucleus is raised to an excited energy state and gives off the excess energy in the form of one or more gamma rays to return to a stable state. The energies of the gamma rays are characteristic of the elements present in the sample. Spectroscopic examination of the induced gamma radiation makes identification and quantitative analysis theoretically possible for most elements. With the exception of ^{4}He, each nuclide of every element can potentially capture neutrons making this technique useful for a vast array of materials.

Certain elements capture neutrons efficiently and decay instantaneously without formation of radioactive products [see Eqn (1.1)]. Some elements also exist that form radioactive products upon neutron capture without decaying through gamma-ray emission [see Eqn (1.2)]. For example, phosphorus and sulfur are pure beta emitters after neutron capture.

This thesis follows the style of the Health Physics Journal.

$$ {}_{1}^{1}H + {}_{0}^{1}n \rightarrow \left[{}_{1}^{2}H \right]^{*} \rightarrow {}_{1}^{2}H + \gamma \quad ; \; {}_{1}^{2}H \; is \; stable \tag{1.1} $$

$$ {}_{1}^{2}H + {}_{0}^{1}n \rightarrow \left[{}_{1}^{3}H \right]^{*} \rightarrow {}_{1}^{3}H + \gamma \quad ; \; {}_{1}^{3}H \rightarrow {}_{2}^{3}He + {}_{-1}^{0}\beta \tag{1.2} $$

Stable ^{2}H is formed in Eqn (1.1) and the radioactive ^{3}H formed in Eqn (1.2) does not decay by a gamma-ray emission. Neither of these elements can be analyzed using traditional NAA techniques. Traditional neutron-activation analysis [also referred to as instrumental-neutron-activation analysis (INAA)] has been very useful in analyzing samples, which form radioactive product nuclei that in turn emit gamma-rays. Also, their cross sections and the daughter's half life must be workable. However, this technique provides marginal analysis of some key elements such as B, Cd and H. Such elements with relatively short-lived daughters, having weak gamma-ray signals or no decay gamma radiation have been successfully analyzed using the Prompt-Gamma, Neutron-Activation Analysis technique.

Prompt-Gamma, Neutron-Activation Analysis (PGNAA) is a method which measures the gamma-rays emitted instantaneously during irradiation. This technique has long been used for analysis of elements not amenable to INAA with the advantage of providing instantaneous and non-destructive measurements. PGNAA has found application in analysis of environmental, medical, geological samples, and in many other fields. PGNAA is most suitable for elements with high neutron-capture cross-sections, whose daughters decay too rapidly. The technique has been demonstrated for various elements using both isotopic and reactor neutron sources.

Reactor-based PGNAA dates back to the work of Isenhour and Morrison (1966a) at the Cornell University TRIGA MARK II Reactor using a modulated neutron beam and a NaI scintillation detector. Because of the poor analytical sensitivities reported by them, the technique was seldom used until later in the 1960's when high energy resolution germanium semiconductor detectors were developed (Belgya and Revay 2004). Reactor-based PGNAA was previously performed as either in-core or out-of-core irradiations. The technique is now generally performed out-of-core, with a beam of neutrons extracted through a beam port. The neutron fluence rate is much lower for out-of-core applications resulting in longer irradiation times than for samples irradiated inside the reactor core. However, the gamma-ray detector can be placed closer to the sample to partially compensate for the sensitivity loss. An extensive review of in-core and out-of-core applications, as well as a list of reactor-based facilities involved in PGNAA studies, is reported by Anderson et al. (1981a, 1981b).

Solid-state detectors and scintillation detectors have been used for PGNAA applications. Although NaI detectors provide excellent advantages of durability, shock resistance, and the ability to operate in a wide range of temperatures, humidity and pressures, solid-state semiconductor detectors provide better resolution compared to NaI detectors. Resolution of peaks is more important than efficiency and high-purity germanium detectors (HPGe) are ideal for the high-sensitivity analysis required in PGNAA (Alfassi and Chung 1995). Energy resolution, the measure of the detector ability to distinguish closely spaced lines in the spectrum, is a function of photon energy and usually described by the full width of the peak at one half of the maximum value. To

determine the peak area reliably, the efficiency must be known adequately (Belgya and Revay 2004) and with certainty to determine reaction rates for quantitative analysis of nuclide concentration.

Multi-elemental analysis using PGNAA is possible through the knowledge of the radioactive emissions and radioactive decay paths for each element. Using this information, the emission spectra of radioactive samples can be analyzed to determine isotopic concentrations. Samples from material science, geology, mining, food analysis, environment studies, and medicine, often have elements like boron, sulfur, and nitrogen in trace quantities. These elements do not form neutron capture products that allow use of traditional NAA, hence these elements are candidates for PGNAA.

Prompt-gamma-neutron activation analysis facilities using rector neutrons have been developed and operated in the US and worldwide. Notable in the US are the National Institute of Standards and Technology (NIST), the University of Missouri Research Reactor (MURR), and the University of Texas reactor in Austin. Major facilities abroad include: JAERI in Japan, the Budapest Neutron Center in Hungary, the KAERI facility in Korea, and DINR, in Dalat, Vietnam. An extensive review of neutron-capture, gamma-ray facilities is provided elsewhere (Lindstrom and Revay 2004).

An attempt was made to develop a working PGNAA facility at the Nuclear Science Center (NSC) reactor of Texas A&M University in the early 90's for use in measuring absorption-cross-section values of geologic core samples provided by Texaco, Inc. (Krohn 1992). The results obtained did not compare well with other

facilities due to low neutron fluence and high gamma-radiation background from the reactor, poorly collimated beam and shielding materials, and the lack of a highly efficient detection system with associated electronics.

The purpose of this research was to investigate the problems with developing a PGNAA facility at the NSC to complement its existing NAA capabilities. This research develops a theoretical model which can predict the net peak area counts expected at a gamma-ray line for a given sample mass under certain experimental conditions. This model would be compared with experimental results. To achieve this goal, computations were carried out using the adopted PGAA Database files of the IAEA Coordinated Research Project for the Development of a Database for PGNAA (IAEA 2003). This database was used in conjunction with the neutron fluence rate measured at BP #1 and the measured detector efficiency. A PGNAA experimental facility was set up at NSC Beam Port #1 and the results of the experimental measurements were compared to the results from the theoretical calculations.

CHAPTER II

THEORY

PGNAA FUNDAMENTALS

PGNAA is used to analyze nuclide concentrations in samples by detecting the gamma rays emitted upon neutron capture. The capture reaction, commonly represented as the (n, γ) reaction in Eqn (2.1) is illustrated in Fig. 2-1:

$$ {}_{Z}^{A}X + {}_{0}^{1}n \rightarrow {}_{Z}^{A+1}X^{*} + \gamma \quad \text{or} \quad {}_{Z}^{A}X(n,\gamma){}_{Z}^{A+1}X^{*}. \tag{2.1} $$

The parent nuclide ${}_{Z}^{A}X$ absorbs a neutron ${}_{0}^{1}n$, to produce an excited nucleus, ${}_{Z}^{A+1}X^{*}$ with emission of the prompt gamma radiation, γ.

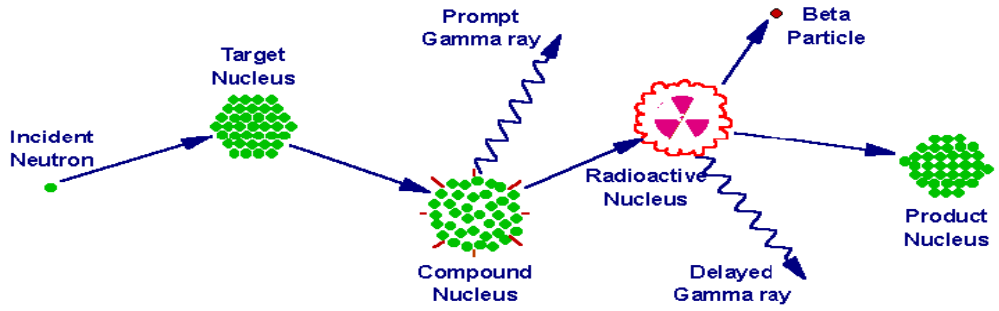

Fig. 2-1. Diagram illustrating the process of neutron capture by target nucleus. (Glascock; http://archaeometry.missouri.edu/naa_overview.html).

Besides radiative neutron capture, another useful reaction is the (n, α) reaction. Following neutron capture, some light elements emit a charged particle, sometimes along with gamma radiation. An important example of this reaction is for boron whose absorption reaction is:

$$^{10}_{5}B + ^{1}_{0}n \rightarrow ^{7}_{3}Li + ^{4}_{2}He + \gamma(478keV). \qquad (2.2)$$

Approximately 6% of the time, the ^{7}Li atom is formed in the ground state, but 94% of the time, the ^{7}Li atom is left in the excited state. The cross section for this reaction is very high, 3837 barns, with a 478-keV gamma-ray produced by the ^{7}Li* nucleus 94% of the time. The recoiling ^{7}Li atom decays in flight, and its gamma rays produce a Doppler-broadened peak that is very easy to recognize (Fig. 2-2).

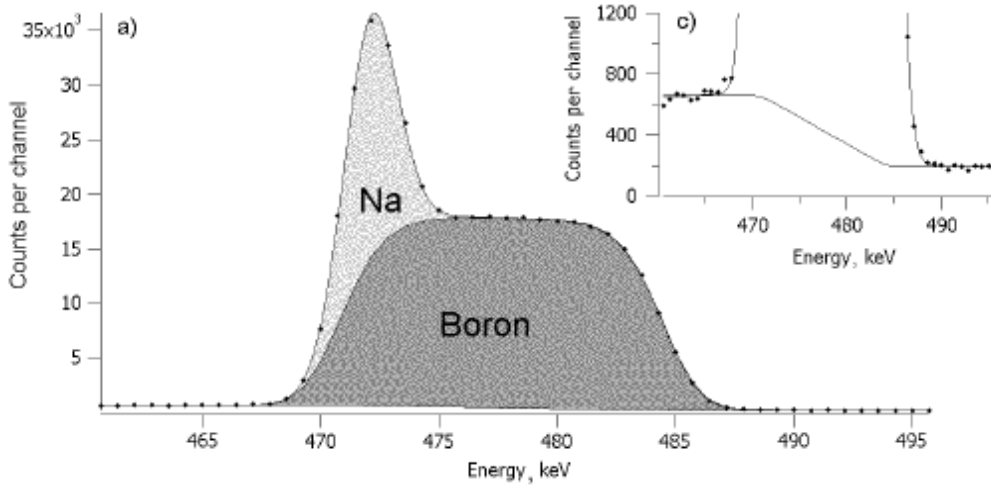

Fig. 2-2. Characteristic shape of boron peak showing Doppler-broadening. (Szentmiklosi et al. 2007).

The characteristic prompt-gamma peaks can better be explained using the energetics of the neutron capture process. When a nucleus absorbs a neutron, a gain in binding energy of the captured neutron raises the resulting compound nucleus to an excited energy state. The excited compound nucleus typically releases the energy in the form of gamma rays. The emission usually takes place through a cascade of two or more photons via intermediate levels to the ground state of the daughter. The intensity of a prompt-gamma ray is determined by the branching ratios of the given and preceding transitions and it is characterized by the emission probability, which is the fraction of the emitted gamma per capture. The emitted photon and the recoil nuclei travel in opposite directions. The excitation energy of the compound nucleus can appear as a single photon of energy equal to the excitation energy of the compound nucleus less a small amount of recoil energy; or as a cascade of several photons whose energies sum to the excitation energy less recoil energy. For energy conservation, the energy of the emitted photon(s), $E\gamma$, and that of the recoil nuclei, E_R, always sum to that of the transition, E_T, as shown in Eqn (2.3).

$$E\gamma = E_T - E_R \qquad (2.3)$$

The excited nucleus returns to the ground or lower energy state emitting decay gamma rays or particles. These secondary processes are also used for quantitative analysis of the sample, which, in most cases, offer better sensitivities than the prompt gamma lines for example aluminum and sodium.

The prompt-gamma rays emitted during de-excitation can be used in identification of component elements. The gamma emissions from compound nuclei

after neutron capture are unique to each element. Assay of the prompt-gamma-rays with a gamma-ray spectrometer provides the basis for identification and quantification of elements and isotopes: the distinct energy signatures identify the component nuclides in the sample and the intensity of the emitted gamma rays is directly proportional to the concentration of the respective nuclides in the sample.

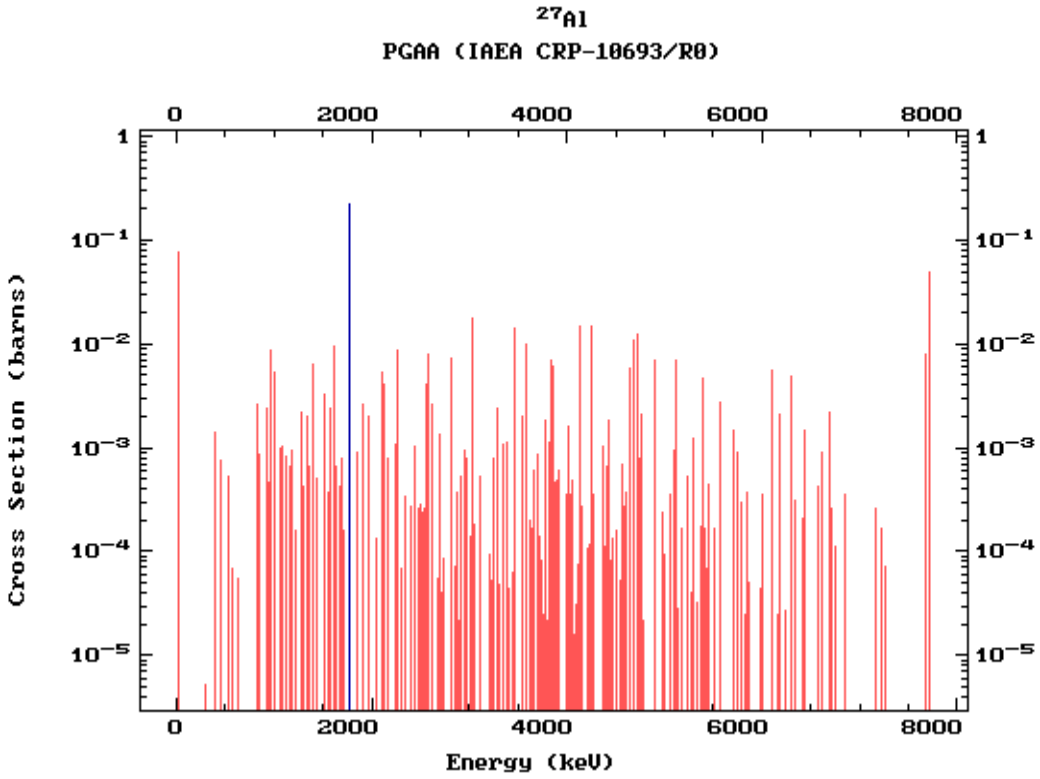

Fig. 2-3. Prompt-gamma spectrum of ^{27}Al. (IAEA 2002; http://www-nds.iaea.org/pgaa/pgaa7/index.html).

The prompt photons are emitted within 10^{-14} to 10^{-12} seconds after formation of the excited nucleus and normally considered instantaneous. Because some atoms release all of their energy through one high-energy gamma ray and others emit a series or cascade of gamma rays, each of these possible gamma rays will appear in the spectrum making the prompt-gamma-ray spectrum complicated. The prompt gamma-ray spectrum of aluminum, for example is shown in Fig. 2-3. The complex spectrum offers the advantage of having several possible gamma lines that may be used singly or in combination to identify and confirm the existence of a given nuclide.

One of the obstacles in establishing the PGNAA technique as a standard nuclear analytical method was the lack of an accurate and complete analytical library (Molnar 2000). Databases now exist that provide information on the most intense gamma-ray lines for each nuclide or element making it easier to identify an element using one or more of its gamma lines (Revay et al. 2004).

NEUTRONS FOR PGNAA

Neutrons for PGNAA applications can come from reactors and non-reactor sources such as accelerators and radioisotopic neutron emitters. Portable neutron sources have been used previously for PGNAA applications, particularly in the field. While offering a wide range of industrial and field applications, non-reactor neutron sources offer low analytical sensitivities when compared to reactor neutron sources. Because of the higher neutron fluence rates, reactor sources offer higher sensitivities.

The energy distribution of reactor neutrons is broad, with about two-thirds of the neutron energies between 0.5 to 3 MeV. A typical research reactor neutron spectrum is shown in Fig. 2-4.

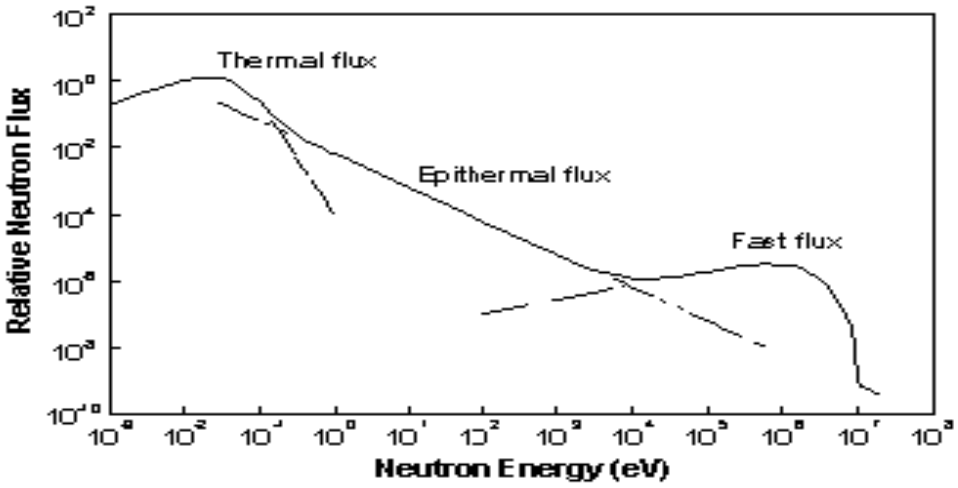

Fig. 2-4. Schematic of reactor neutron spectrum. (Lindstrom and Revay 2004).

As can be seen in the figure, neutron energies are broken into three broad regions: thermal, epithermal and fast are used to describe the neutron energy regions. Because neutron capture cross sections are much larger at lower energies, thermal or cold neutrons have been most useful for PGNAA applications (Lindstrom and Revay 2004).

The ground work for high-resolution reactor PGNAA can be traced to the published works of Isenhour and Morrison (1966a, 1996b). A review of the fundamental contributions leading to PGNAA is provided by Lindstrom and Anderson (1985).

Factors that determine the applicability of neutron capture for any given element have been identified by (Glascock 1981) to include:

- The capture cross section of the target nucleus;
- Number of incident neutrons; and
- Characteristic of various capture products such as half-lives and gamma-ray intensities.

The general equation for activity, A of an element with cross section, σ, irradiated by thermal neutrons of fluence rate , Φ , over time, T_i, is given as:

$$A = N\Phi\sigma(1 - e^{-\lambda T_i}) \times (e^{-\lambda T_d}) \qquad (2.4)$$

where:

N= number of atoms of the target nuclide;

λ = radioactive decay constant for the radionuclide produced; and

T_d = decay time.

The gamma radiation from nuclear states excited by neutron capture is analyzed instantaneously. Half-lives for capture-gamma rays are very short, typically 10^{-14} to 10^{-15} seconds, so the decay constants are about 10^{15} s^{-1}. For irradiation of practical duration, the term $(1 - e^{-\lambda T_i})$ = 1. The decay time is zero, so, $e^{-\lambda T_d}$ =1. The prompt gamma emission rate in PGNAA reduces to

$$A = N\Phi\sigma. \qquad (2.5)$$

Thus, the requirement for PGNAA elemental analysis is a reaction cross section sufficiently large to produce measurable capture-gamma-ray activity for a given beam

intensity. Also, the gamma-ray peak should be resolved from the rest of the complex PGNAA spectrum (Lombard et al. 1968).

While gamma lines of given energies are used to identify elements, partial gamma-ray production cross sections, σ_γ, given in Eqn (2.6) are also used.

$$\sigma_\gamma = f\sigma P_\gamma . \tag{2.6}$$

where:

f =the natural abundance of the isotope in the element;

σ = isotopic capture cross-section; and

$P\gamma$ = the emission probability of the gamma ray with the given energy which gives the fraction of the emitted photons per capture. Thus

$$A_\gamma = N\Phi\sigma_\gamma . \tag{2.7}$$

The elemental emission probability, which is the emission probability weighted by the isotopic abundance, can also be expressed as the ratio of the partial gamma-ray production cross section to the total capture cross section. The partial gamma-ray production cross section characterizes the probability of producing a given gamma-ray energy for an atom of the element under irradiation. By knowing $A\gamma$, σ_γ and Φ, the number of atoms, N, of a particular element can be calculated. The partial gamma-ray production cross section depends largely on the neutron energy. Thermal or cold neutrons with energies ≤ 0.4 eV, provide increased average probability for interaction at lower neutron velocities, which favor prompt-gamma, neutron-activation analysis.

To satisfy the neutron beam criterion highly suitable for PGNAA, modern developed reactor facilities employ filtration using crystals of appropriate orientation, mirror-guided beams, or Bragg diffraction using polychromatic crystals (Byun et al. 2002). The removal of epithermal and fast neutrons from the beam was attained using combinations of filtration and diffraction at the MIT facility (Harling et al. 1993).

The use of perfect single crystals of various materials as filters for thermal neutron beams has long been established and the percentage transmission, T_n, investigated. According to Adib et al. (2005), a 7.5-cm-thick sapphire with a 1-0-0 orientation is sufficient for removing neutrons with energies > 1 eV (Tn < 8%) while providing high transmission (Tn > 85%) for neutron energies < 0.02 eV. This shows that a 7-cm-thick sapphire mono-crystal can be successfully used to transmit thermal neutron fluence having a Maxwellian distribution with neutron gas temperature close to 300 K, while significantly rejecting the accompanying slowing down component (dE/E) with neutron energy E > 1eV. An improvement of ≈ 5% neutron transmission at neutron energies < 0.02 eV (cold neutrons) through a cooled sapphire crystal at LN_2 temperature was also reported (Adib et al. 2005). A sufficient fluence of thermal neutrons was obtained by means of fast neutron and gamma-ray filtering using a sapphire crystal at the NIST facility (Anderson and Mackey 2005, Mackey et al. 2004). A silicon crystal was used at the University of Missouri, Columbia (Hanna et al. 1981).

GAMMA-RAY DETECTION

Nuclei formed in capture reactions release prompt-gamma rays with energies ranging from about 30 keV to over 12 MeV. To make the analysis practical, a very efficient gamma-ray spectrometer with high resolution is required. Gamma-ray spectrometers used for PGNAA now include data acquisition and analysis systems to provide information on activity and energy of the prompt-gamma peaks required to determine the sample composition (Belgya and Revay 2004). Low detection efficiency of the resulting gamma-rays will result in low analytical sensitivity.

The prompt gamma-ray counting rate of a particular energy line or peak in the spectrum at a given energy is given by the relation:

$$C = \frac{mN_a}{M}\Phi\varepsilon(E_\gamma) f\sigma P_\gamma = \frac{mN_a}{M_a}\Phi\varepsilon(E_\gamma)\sigma_\gamma . \qquad (2.8)$$

where:

C= the gamma-ray counting rate of a particular energy line;

m = mass of the element;

f = isotopic abundance of the capturing isotope of the element of interest;

N_a= Avogadro's number;

M_a= the atomic weight of the element;

σ = microscopic capture cross-section for the element;

ε = gamma-ray detection efficiency for the energy line;

Φ = neutron fluence rate incident on sample of mass m; and

P_γ = emission probability of the gamma ray with the given energy, which is the fraction of the photons emitted per capture.

From Eqn (2.8), it follows that the recorded count rate depends on the product of the interaction cross-section, the isotopic abundance of the target nuclei, and the gamma-ray yield associated with the reaction. Higher values of the product of these quantities results in higher sensitivity for the particular isotope and hence a lower detection limit.

The counting efficiency of an HPGe , i.e., the ratio of the number of pulses recorded to the number of gamma rays emitted by the source, depends on sample geometry and the gamma-ray energy. The absolute efficiency includes the effect of the solid angle subtended by the detector measured to the surface of the crystal, not the detector housing. For PGNAA experimental conditions, gamma-ray emission from the sample can be considered isotropic. Neglecting attenuation effects between the source and detector, the number of photons in the photopeak N, over a period of time T is

$$N = \frac{S\varepsilon_{ip}\Omega}{4\pi}T. \qquad (2.9)$$

where:

S= number of photons emitted by the source over time T;

ε_{ip}= intrinsic peak efficiency of the detector; and

Ω= the solid angle (in steradians) subtended by the detector at the source position (Fig. 2-6).

The solid angle subtended by the detector at the source position is defined as

$$\Omega = \int_A \frac{\cos\alpha}{d^2} dA. \qquad (2.10)$$

where:

r = the distance between the source and surface element, dA, and

α = the angle between its normal and the source direction.

A second integration is required for cases in which the volume of the source is not negligible. Considering the typical case, where the source is located at distance, d, along the axis of a right-circular-cylindrical detector of radius, a, (See Fig. 2-5), the solid angle is expressed as:

$$\Omega = 2\pi\left[1 - \frac{d}{\sqrt{d^2 + a^2}}\right]. \qquad (2.11)$$

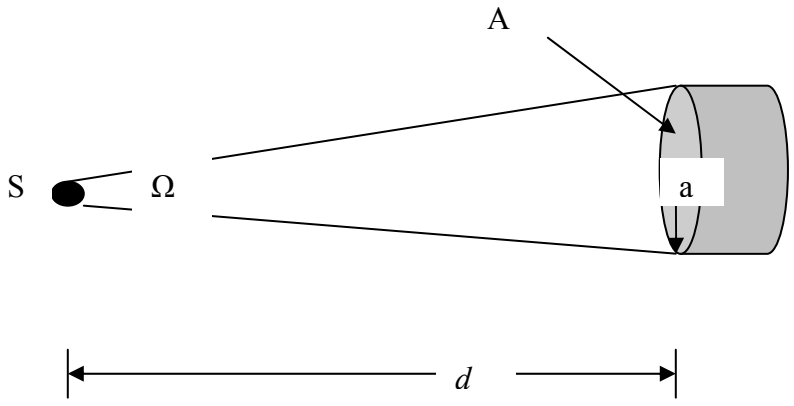

Fig. 2-5. A point source along the axis of a right circular cylindrical detector. (Knoll 1999).

For d>>a, the solid angle reduces to the ratio of the detector plane frontal area, A , visible at the source to the square of the distance thus:

$$\Omega = \frac{A}{4\pi d^2} = \frac{a^2}{4d^2}. \qquad (2.12)$$

To be detected, the photon must transfer part or all of its energy by one of the three interaction modes-photoelectric effect, Compton scattering or pair production. For a count to be recorded within a full energy photopeak, all of the photon energy must be deposited in the active volume of the detector either as a single photoelectric event or by multiple events, for example, Compton followed by the scattered Compton photon having a photoelectric event.

N-type and p-type detectors have been used for PGNAA, but with different responses especially below 100 keV. For a similar active volume, the p-type (GEM) has a thicker outer contact, which contrasts with the much thinner contact of the n-type (GAMMA-X) HPGe. In most cases, the end cap of the n-type HPGe is made of a material with high transmission at low energies such as beryllium metal foil or carbon fiber foil. This makes the detection efficiency for p-type detectors fall off sharply below about 150 keV, as shown in Fig. 2-6.

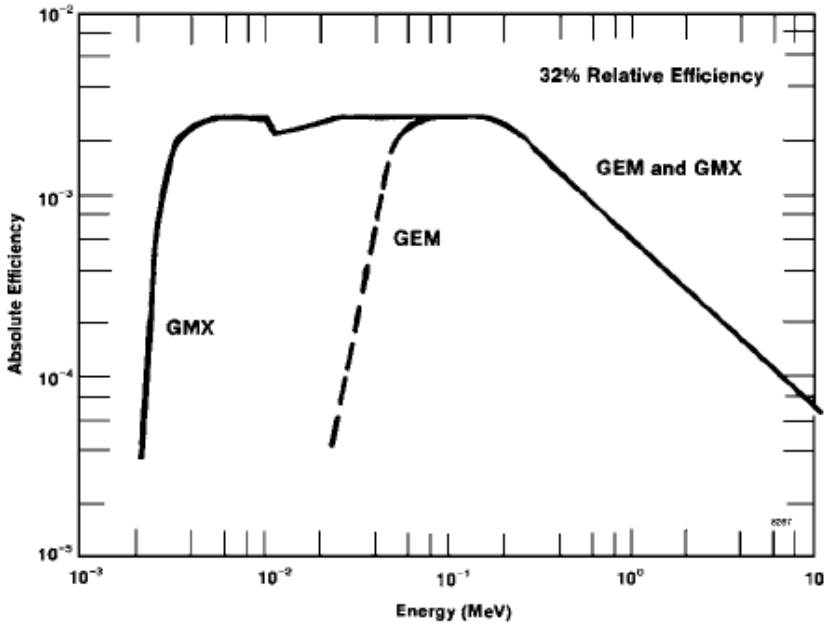

Fig. 2-6. Absolute efficiency vs. energy for 32% GEM and GAMMA-X HPGe coaxial detectors. (EG&C, Ortec. www.ortec-online.com/detectors/photon/pdf/).

Thus, gamma rays from elements with energies in this range cannot be measured accurately. The low energy efficiency of the n-type HPGe is increased because of the reduced thickness of the dead layer. Fast neutrons affect the performance of germanium detectors by degrading the resolution. P-type HPGe detectors are more susceptible to neutron radiation damage than the n-type, especially for detectors with lower relative efficiencies. N-type detectors are more easily repaired for neutron radiation damage than the p-type. N-type detectors are the most preferred for PGNAA applications.

Efficiency calibration of gamma-ray detectors over a wide range of PGNAA energy spectra has been noted as an important requirement for the technique. Attempts

were made to determine the absolute efficiency of detectors using various calculations at the Budapest PGNAA facility. (Molnar et al. 2002). This method is inconvenient for routine analysis due to the numerous parameters involved. Preference is given to the use of gamma-ray sources with known disintegration rates. Standard calibration sources with known activities have been used from low energies up to about 1.5 MeV, while (n, γ) sources with known reaction rates have been use for higher energies. A formula given by (Molnar et al. 2002) is:

$$\varepsilon(E_\gamma) = \frac{C_\gamma}{NP_\gamma} K = \frac{R_\gamma}{AP_\gamma} K \qquad (2.13)$$

where:

C_γ = measured net peak area counts;

R_γ = count rate, i.e., the peak area in unit time;

P_γ = emission probability of the corresponding gamma-ray;

K = correction factors for losses during acquisition;

N= number of disintegrations; and

A= activity, or number of disintegrations per unit time.

QUANTITATIVE ANALYSIS

Elemental identification of PGNAA spectra and quantitative analysis are two most important applications of this technique. Nearly every neutron capture yields gamma

rays that may potentially be used to identify the capturing element. Neutron-capture gamma rays have higher energies than decay gamma rays. The energy spectrum of capture gamma rays from most nuclides is fairly complex and further complications may arise from gamma rays emitted from shielding materials. In addition to the large number of prompt-gamma rays (full energy peaks), single and double-escape peaks from the high-energy gamma rays populate the spectra, leading to more complex gamma-ray spectra than observed with decay gamma rays. This renders peak analysis for elemental identification very complex. In the PGNAA technique, elements are identified by their gamma-ray lines and quantified by the radiation intensity. Peak assignments for elemental identification of the measured gamma-ray spectra are carried out by comparing the results from the spectrum evaluation with known prompt-gamma-ray data. A comprehensive database has been developed for this purpose, courtesy of the Coordinated Research Program of the International Atomic Energy Agency (IAEA 2003). This is the one of the most current and standardized tabulation of gamma-ray energies and intensities.

ABSOLUTE METHODS

The neutron capture reaction rate equation can be written as

$$R = N\sigma\Phi. \qquad (2.14)$$

where:

R = reaction rate (sec^{-1});

σ = neutron capture cross section at the given energy (barns);

Φ = neutron fluence (neutrons/cm^2-sec); and

N = number of atoms of the desired nuclide in sample.

For a given gamma-ray energy of partial gamma-ray production cross-section, σ_γ, the count rate, C_γ, of a gamma peak at a given energy in the spectrum can be written as:

$$C_\gamma = \varepsilon(E_\gamma) n \sigma_\gamma \Phi . \qquad (2.15)$$

where:

$\varepsilon(E_\gamma)$ is the energy-dependent counting efficiency of the gamma-ray detector.

Equation (2.15) holds for a monochromatic beam of neutrons and an ideally thin and homogenous sample. This is very much an issue for neutron spectra from filtered and guided beams due to absorption of neutrons at certain energies by a filter and diffractometer (Yonezawa 2004). Taking into account the non-homogeneity of the sample, the neutron-energy distribution and the energy-dependence of the cross section, the count rate of the gamma peak can be expressed as:

$$C_\gamma = \int_V \int_0^\infty \frac{\mu(r)}{M} N_A \sigma_\gamma(E_n) \Phi'(E_n, r) \varepsilon'(E_\gamma, r) dE_n dr . \qquad (2.16)$$

where:

$\mu(r)$ = the mass density of the examined element as a function of position r in the sample (accounting for the non-homogeneity of the sample);

M = the atomic mass of the element, N_A is the Avogadro's number;

$\sigma_\gamma(E_n)$ = the partial gamma-ray production cross section for the given gamma ray as a function of the neutron energy;

$\Phi'(E_n, r)$ = the neutron fluence rate as a function of energy and position within the sample to account for non-homogeneity of the beam and self shielding and scattering; and

$\varepsilon'(E_\gamma, r)$ = the energy and position dependent counting efficiency of the detector, to account for gamma self-absorption as well as the geometric efficiency (Yonezawa 2004).

In theory, elemental concentrations in a sample under investigation, i.e., the number of atoms, *n*, can simply be determined from Eqn (2.15) and by extension Eqn (2.16). This is the absolute method of quantitative estimation. In practice, neutrons have an energy distribution with energy-dependent cross sections and the samples are not homogenous; the absolute method becomes inadequate for precise analysis due to difficulties in obtaining accurate neutron spectra, accurate neutron cross section functions, the detection efficiency and gamma-ray emission probabilities.

In view of these difficulties, elemental concentrations are usually determined using relative and internal standardization methods. INAA uses a comparator method based on standards to determine concentrations of elements in samples. A similar technique is used widely in PGNAA analysis of elemental concentrations.

RELATIVE AND INTERNAL STANDARDIZATION METHODS

The relative standardization method seeks to determine the elemental concentrations by comparing gamma-ray peak count-rates of the element in the sample with that of a known standard. The method compares the analytical sensitivities of a known mass, M_{std}, of an element in a standard sample with an unknown mass, M_u, of the same element in a test sample related to the gamma-ray production rates for each of the samples tested, i.e.,

$$\frac{M_{std}}{C_{std}} = \frac{M_u}{C_u} \tag{2.17}$$

where:

C_{std} = peak count-rates of known standard; and

C_u = peak count-rate of unknown element in sample.

Since the specific count rate, i.e., the analytical sensitivity for the element of interest is constant, the mass of the element in the analyte is obtained mathematically from equation (2.17). The product of the neutron-capture reaction rate and the gamma-ray emission probability, which is difficult to obtain using the absolute method, can be eliminated by measuring known amounts of elements under similar conditions as the sample.

The internal standardization method, sometimes called the ratio or k_0 method, eliminates differences in chemical composition and geometrical conditions between the samples and standards using the relative standardization method. The technique is called

the k_0 method because it is equivalent to a similar method used in traditional NAA. During sample irradiation, there may be variations in the fluence rate, which will vary the reaction rate. To eliminate the effect of fluence rate variation, a ratio-based analysis can be performed. Through judicious choice of standards, sources of uncertainty from cross sections, yield, detector efficiency and neutron fluence rate can be eliminated by working with ratios. Since hydrogen has only one capture gamma-line, and is also a cross section standard, it has been used as a comparator element most often. The ratio of count rates from two different energy peaks will eliminate the effect of fluence rate variation. The effects of yield and efficiencies can be eliminated by working with ratios of same energy peaks from two different samples, one of which can be a standard. Accurate detection efficiency calibration of the detector is essential in this method. A more detailed review of quantitative analysis using the k_0 method in PGNAA is presented elsewhere. (Yonezawa et al. 2004, Molnar et al. 1998).

CHAPTER III

EXPERIMENTATION AND PREDICTIVE MODEL

The (PGNAA) facility developed for this study is located at Beam Port # 1 on the Lower Research Level (LRL) of the Nuclear Science Center Reactor. This beam port has ample space around it to accommodate all design components. The Nuclear Science Center (NSC) at Texas A&M University houses a 1 MW TRIGA pool-type reactor with extensive capabilities for radiation research. The reactor pool has a semi-circular stall of radius 1.37 m (4.5 feet) at one end with various beam ports, through tubes and a thermal column as shown in Fig 3-1. The primary ports, designated as Beam Ports #1 and #4, are situated on the south and north ends of the pool, respectively. Between the beam ports, there is a graphite-filled coupler box, which is part of another experiment at the thermal column. The flanged-off faces of the beam ports are in contact with the sides of the coupler box allowing the neutrons to escape through the ports. The neutron beam is controlled by a water shutter, which prevents the passage of the neutron beam when filled with water. The shutter is controlled by a switch near the beam port. The shutter is opened by pressurizing a section of the beam port with compressed air to remove the water. The shutter will re-flood when the airflow stops. Neutron fluence out of Beam Port #1 consists of neutrons leaking from the graphite in the coupler box. This avoids direct-fission gamma rays coming from the reactor core and allows a highly-thermalized neutron beam to exit from the port.

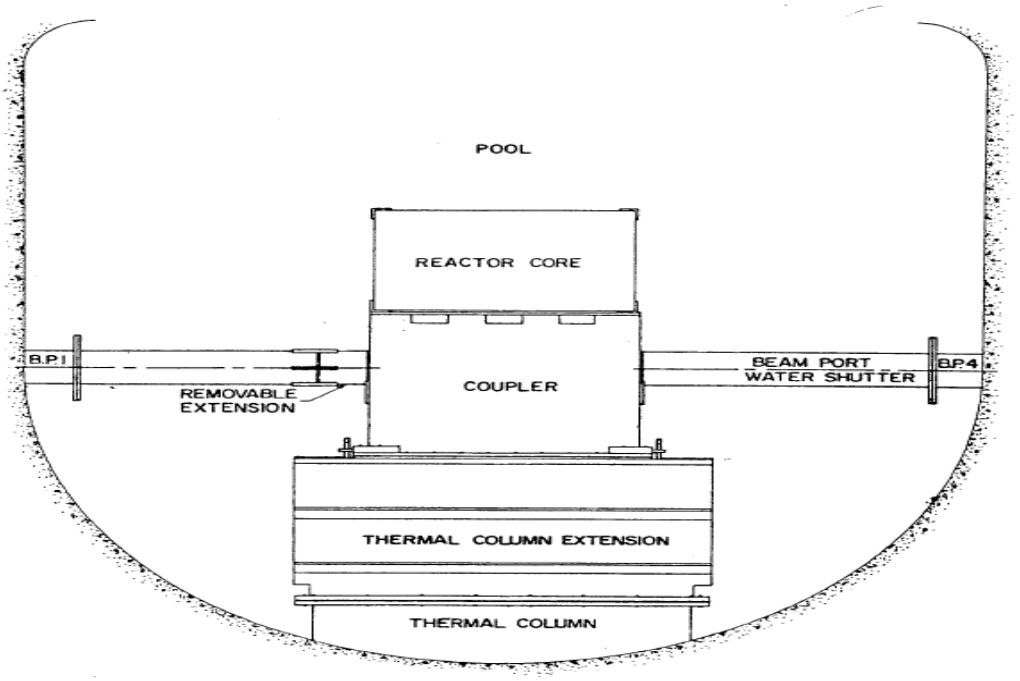

Fig. 3-1. Beam Port locations in the NSC reactor pool showing BP#1. (Krohn 1992).

The NSC reactor has a unique arrangement to moderate neutrons coming from the reactor core. The graphite-filled coupler box between the beam ports has minimal clearance between the flanged-off faces of the beam port and the sides of the coupler box. This arrangement minimizes the presence of water that would absorb part of the neutron fluence rate.

PRELIMINARY BEAM CHARACTERIZATION

The first task was to determine the neutron fluence rate and beam-energy composition to ensure that the beam is suitable for PGNAA. For radiological safety, temporary shielding was built around the beam port to stop the neutrons and attenuate the reactor gamma-rays. A concrete wall, 2.1-meters high (7-feet) and 0.38-meters thick (15-inches) was erected about 92 cm (3 feet) in front of BP#1 to absorb neutron radiation. An additional 10-cm (4-inches) layer of lead bricks was stacked behind the concrete wall to attenuate both reactor gamma rays as well as capture gamma rays from the concrete and air.

Following standard practice for mixed radiation fields, the order of shielding materials from the source was concrete followed with lead, in the order of increasing atomic number, Z. The temporary shielding arrangement is shown in Fig. 3-2. Beam Port #1 had previously been used for neutron depth profiling (NDP) experiments at the NSC (Khalil 1989). During the initial beam characterization measurements, the temporary shielding was sufficient to keep the exposure rates from neutrons and gamma radiation to 0.2 mSv h^{-1} (20 mrem h^{-1}) and 0.1 mSv h^{-1} (10 mrem h^{-1}) respectively at the fence shown in Fig. 3-2. Behind the lead shielding, the neutron fluence rate was 4 mSv h^{-1} (400 mrem h^{-1}) as measured with a remball. Gamma-ray exposure rates were measured using a VIC 451-type ionization chamber.

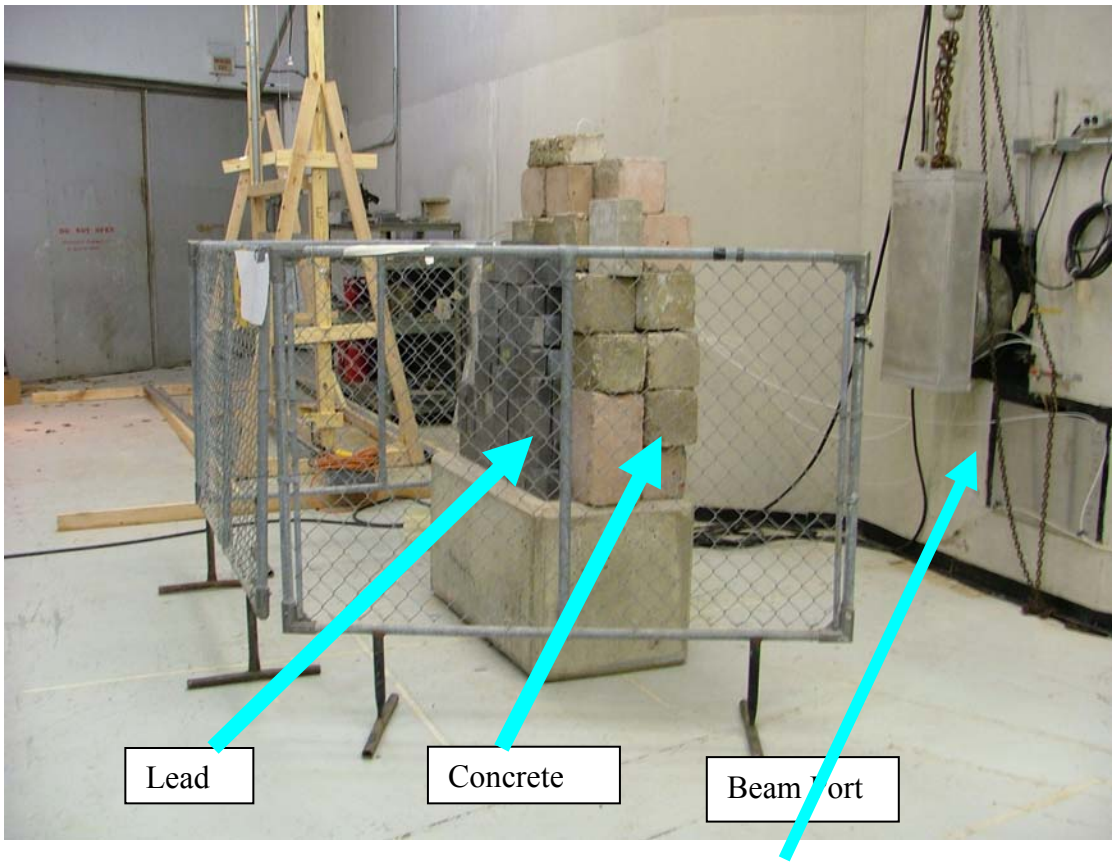

Fig. 3-2. Temporary shielding around Beam Port # 1.

NEUTRON FLUENCE RATE MEASUREMENTS

Several measurements of total neutron fluence were carried out using bare and cadmium-covered gold foils. Naturally occurring gold is 100 % ^{197}Au and has an absorption-cross section of 98.7 barns that provides reasonable activation with short irradiation times. The neutron beam from a nuclear reactor is not monoenergetic. The thermal neutron velocities differ and cross sections vary depending on the neutron

velocity. Gold foil has been used as an activation detector because in the thermal region, its activation cross section, to a good approximation varies inversely with the neutron velocity. Gold also has a large resonance integral so when irradiating the gold foil in a beam with significant epithermal fluence rate, a part of the activity obtained will be from epithermal neutrons. The contributions of the thermal and resonance neutrons are usually determined using the cadmium-difference method. Cadmium has a very large cross section for neutron energies ≤ 0.5 eV. If a gold foil is covered with cadmium of appropriate thickness (about 0.5 mm) thermal neutrons will be fully absorbed by the cadmium so that the activity of the cadmium-covered gold foil will be induced only by epithermal neutrons with energies above the cadmium cut-off energy (about 0.5 eV). By taking the difference between the activities of a bare and cadmium covered gold foil, the thermal neutron and epithermal contributions can be determined and the fluence rate or each calculated. However, corrections may be required for fluence rate depression and self shielding.

The activity induced by thermal neutrons was determined by irradiating two sets of bare and cadmium-covered gold foils. Each gold foil was approximately 0.005 cm thick and the cadmium covers about 0.058 cm thick. Small foil thicknesses would minimize the effects of self shielding. The first set of gold foils weighed 31.9 and 32.3 mg for the bare and cadmium-covered foils respectively. The second set weighed 32.8 and 33.1 mg for the bare and cadmium-covered foils as well. The two sets were irradiated simultaneously for 5 hours within the sample chamber at 80 cm (31.5 inches) and 87 cm (34.5 inches) from the BP #1 collimator. The irradiated foils were assayed

using a standard HPGe gamma spectrometry system. The activity induced in the covered foil was due to epithermal neutrons only. The activity due to the thermal flux was determined as the difference between the bare and cadmium-covered gold foils. The thermal and epithermal neutron fluence rates were calculated from standard reaction rate equations using the activation cross section of gold, the number of atoms of ^{197}Au in the foil, the corresponding activity after irradiation, the irradiation and decay times, and the decay constant of gold. It is also customary to define the cadmium ratio, the ratio of the activities of bare and cadmium-covered foils. A high cadmium ratio is a good indication that the beam is highly thermalized.

An average thermal neutron fluence rate of 8.73×10^6 n cm^{-2} s^{-1} was obtained with an average epithermal fluence rate of 1.11×10^5 n cm^{-2} s^{-1}. Whereas the thermal fluence rate obtained was judged adequate, the epithermal fluence rate and a corresponding cadmium ratio of 5.57 gave an indication that the quality of the beam could be troublesome for PGNAA applications. The foregoing led to attempts to improve the cadmium ratio. The foil activation measurements were repeated after removing all the components in the beam port leaving the cylindrical graphite plug towards the reactor pool end and they confirmed the first measurements. However, the neutron and gamma radiation levels were increased.

The insignificant difference in neutron fluence rates and cadmium ratios, coupled with elevated gamma and neutron radiation levels, forced consideration of other options

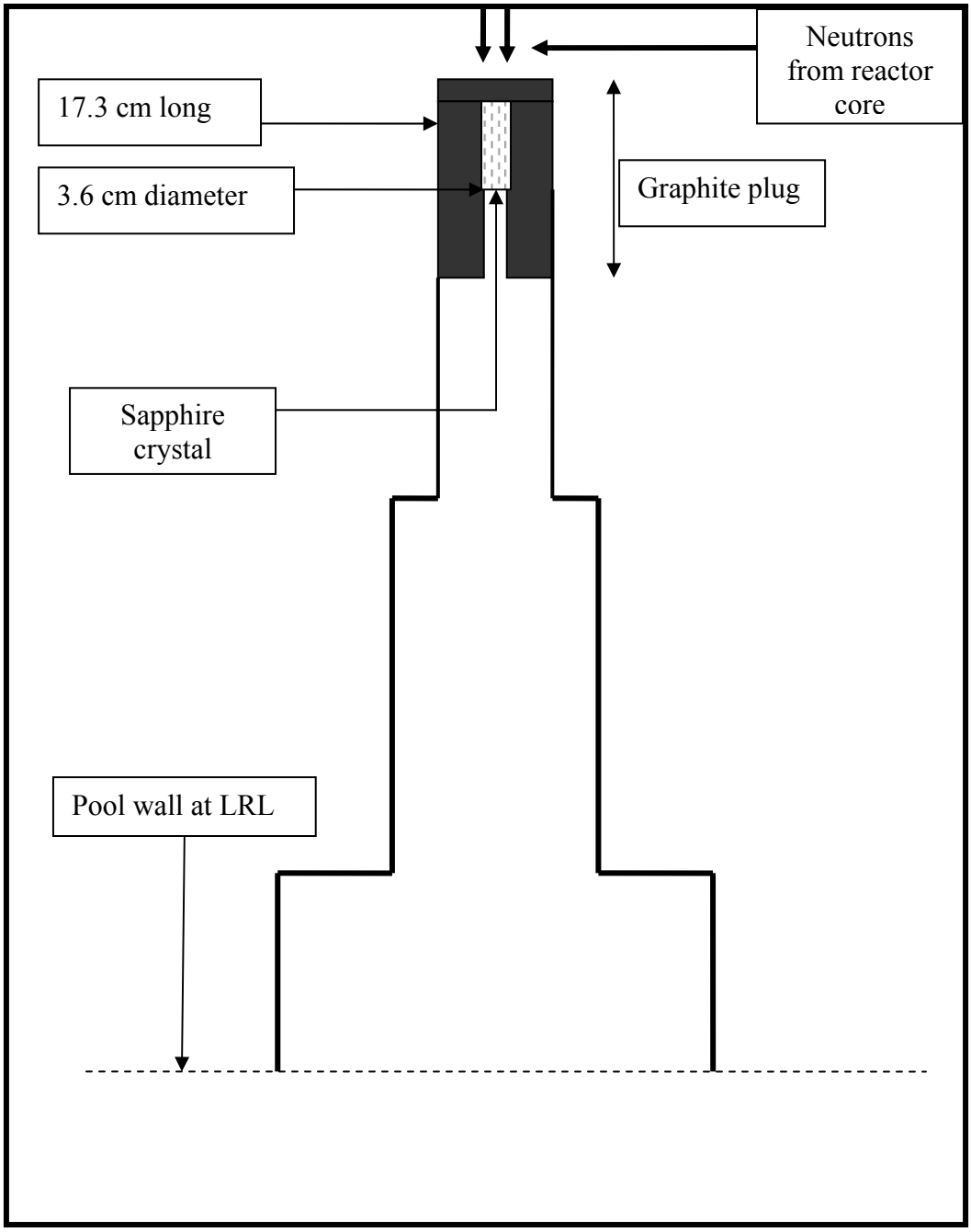

Fig. 3-3. Beam port showing location of sapphire crystal.

to achieve the desired beam quality. Prior to setting up the PGNAA facility, two major modifications were made to Beam Port # 1 aimed at improving the cadmium ratio, lowering the gamma background, and providing a better collimated neutron beam at the opening of BP #1. To achieve this objective, a crystal filter was employed along with a different collimator. A sapphire crystal, 17.27-cm long (6.8 inches), and 3.56-cm in diameter (1.4 inches), was placed in the graphite plug near the reactor pool end of BP #1 as shown in Fig. 3-3. The sapphire crystal was obtained for use in the NDP experiment (Khalil 1989).

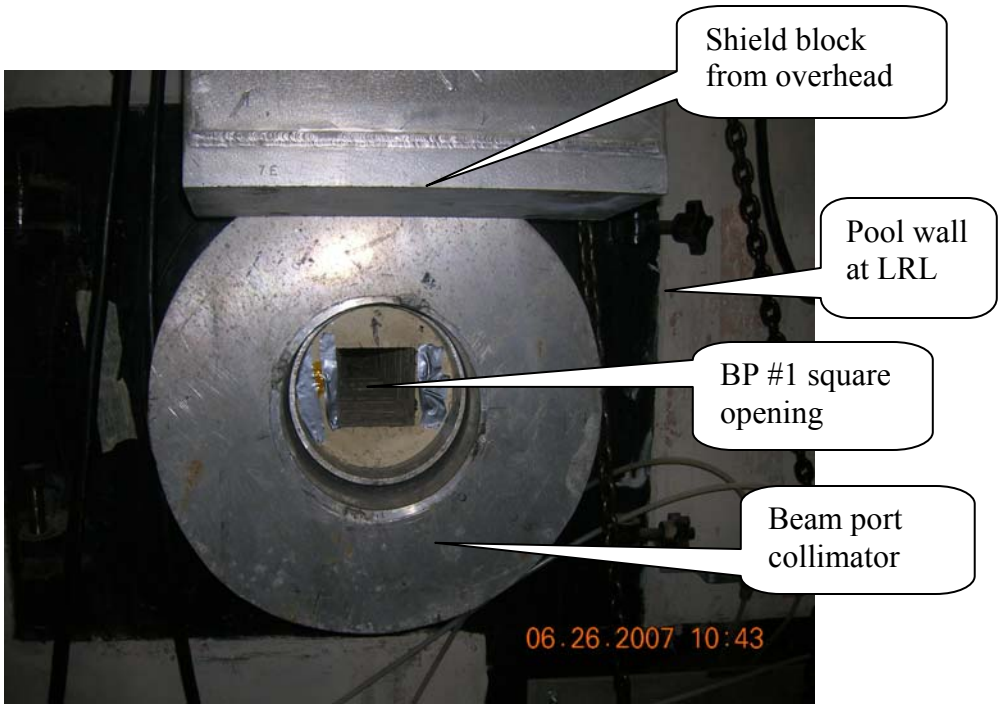

Fig. 3-4. Beam port collimator used for PGNAA.

Also, the collimator inside BP #1 earlier used for the NDP experiment was replaced with another collimator used at Beam Port #4 for neutron radiography. This collimator has a square opening of 9.53-cm (3.75 inches) by 9.2-cm (3.625 inches) as shown in Fig. 3-4. It was inserted from the opening of BP #1 at the LRL. The new collimator would serve to reduce the beam divergence at the beam port opening. Theoretically, the sapphire crystal should transmit sufficient thermal neutrons and a relatively small amount of epithermal and fast neutrons, resulting in a higher cadmium ratio. These modifications reduced the radiation exposure levels on the LRL tremendously. Radiation exposure levels were reduced by a factor of 20. The gamma-radiation level measured at the LRL was less than 0.005 mSv h^{-1} (0.5 mR h^{-1}) while the thermal neutron fluence rate was about 0.02 mSv h^{-1} (2 mrem h^{-1}). Neutron and gamma radiation surveys around the LRL and mezzanine indicated that the levels were well within regulatory and facility administrative limits.

PGNAA EXPERIMENTAL SET-UP

The layout of the experimental setup is shown in Fig. 3-5. The sample position was fixed at 91-cm (36 inches) from the beam port #1 opening. The sample-to-detector distance was 55-cm (21.5 inches) but this could be varied. These distances are a compromise between reduction in gamma rays from the reactor core without a substantial loss in neutron fluence rate, to provide a good signal-to-noise ratio and improved prompt gamma-ray detection efficiency.

The average thermal neutron fluence rate of 9.3 $x10^5$ n cm^{-2} s^{-1} was measured recently around the sample location with an average epithermal neutron fluence rate of 4.58 x 10^2 n cm^{-2} s^{-1}. The neutron beam from the reactor core was filtered using sapphire crystal in the graphite plug towards the core end of the beam port. The effect of this was an improvement in the cadmium ratio from 5.57 to about 122 at the sample position, but with a substantial loss of thermal neutron fluence rate from an initial value of 8.8 x 10^6 n cm^{-2} s^{-1} to 9.3 $x10^5$ n cm^{-2} s^{-1}.

NEUTRON BEAM COLLIMATION

The neutron beam exiting from Beam Port #1 passes through a 5-cm (2-inch) diameter hole in a circular sheet of borated polyethylene. The neutrons traverse a pathway lined on all sides by 5-cm-thick (2-inch) borated polyethylene from the beam port opening. Surrounding all sides of the beam path (except beneath of the borated polyethylene material) are lead bricks, 10-cm (4 inches) thick, followed by approximately 5-cm (2 inches) thickness of paraffin wax. The shielding arrangement around the neutron beam collimation up to the sample chamber and beam stop is shown in Fig. 3-6. Borated polyethylene has about 5 % boron content. The boron captures neutrons and emits 478-keV gamma rays, that are attenuated by the surrounding lead bricks. Any scattered or leaked neutrons from the shielding cracks will be mostly absorbed by the paraffin wax. Surveys for neutron and gamma radiation around this area were well within facility work permit levels.

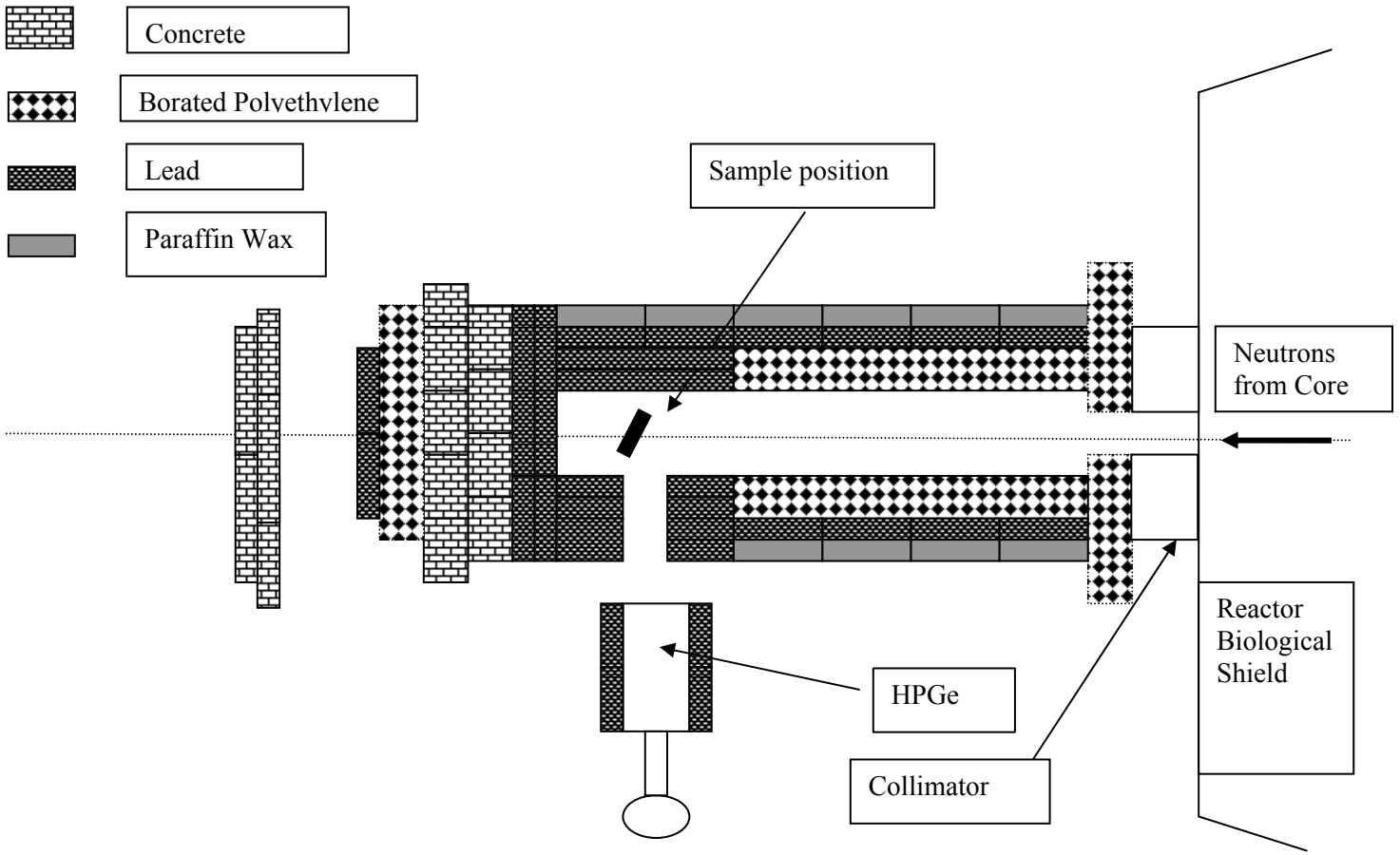

Fig. 3-5. Top view of the PGNAA system component arrangement. (not drawn to scale)

Inside the sample chamber, the use of materials having boron content was minimized and lead bricks were mostly used as construction materials. The intent was to reduce the capture gamma-ray signal from boron. The chamber was completely covered with lead bricks on all sides with a base of borated polyethylene completely covered with lead. The sample chamber had a sheet of lead at the top. This sheet could be removed easily and the chamber opened to change samples.

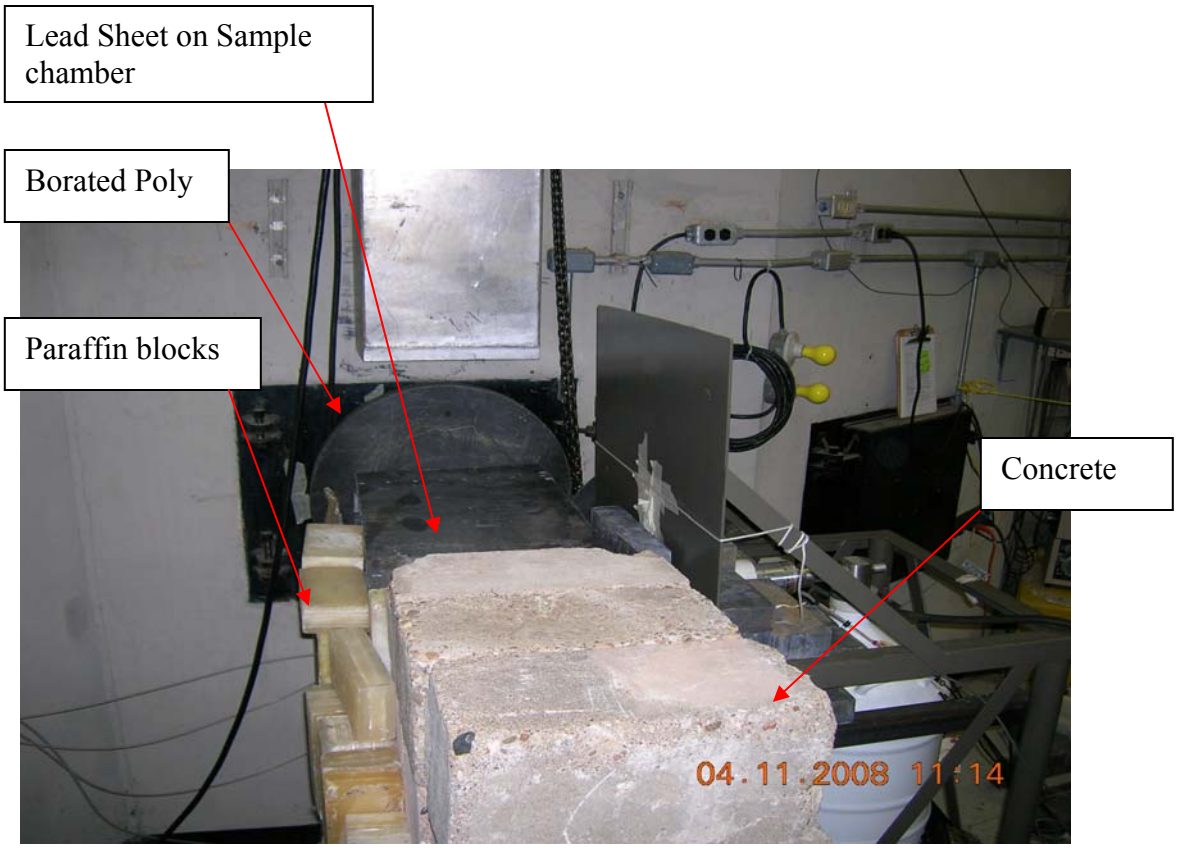

Fig. 3-6. PGNAA facility showing shielding around neutron beam collimator and beam stop.

Lead has a lower capture cross section for neutrons, producing fewer capture-gamma photons than boron. However, the 7.6 MeV capture-gamma radiation from lead still increased the background. Ideally, the shielding materials from beam port opening to the sample position should be made of materials which capture neutrons without emission of gamma radiation. Li-6-based shielding materials, which have this unique property and have been widely used by other facilities, could not be obtained during this phase of the project.

BEAM STOP

Most samples do not absorb the entire incident neutron beam and, in most cases, the beam diameter does not focus completely on the sample due to a smaller sample size. The unused neutrons must be completely absorbed in a manner that will not elevate the gamma-radiation exposure in the facility, increasing the detection background around the experiment. The beam stop is made of lead, followed by concrete, borated polyethylene, and, finally another layer of lead bricks. The multilayered shielding approach ensures absorption of any unused neutron radiation, while attenuating gamma radiation originating from the reactor core, sample, and shielding materials. While the design was not perfect, it was sufficient.

DETECTION SYSTEM & ACQUISITION ELECTRONICS

The gamma-ray detection system consists of an Ortec GEM series High Purity Germanium coaxial detector system (Model No GEM-23185-P) with a 17.8 % relative efficiency. It has crystal diameter and length of 54.6 x 49.5 mm and a resolution of 1.9 keV at 1.33 MeV energy of ^{60}Co. The quality assurance data sheet for the HPGe is enclosed in Appendix F. It has a pop-top cryostat configuration and an in-built preamplifier. The HPGe has a horizontal cryostat with an extended 6-cm diameter end cap mounted in an off-set necked Dewar. The cryostat is mounted perpendicularly to the incident neutron beam at a distance of 55 cm (21.5 inches) from the sample position on steel frame rollers as shown in Fig. 3-7.

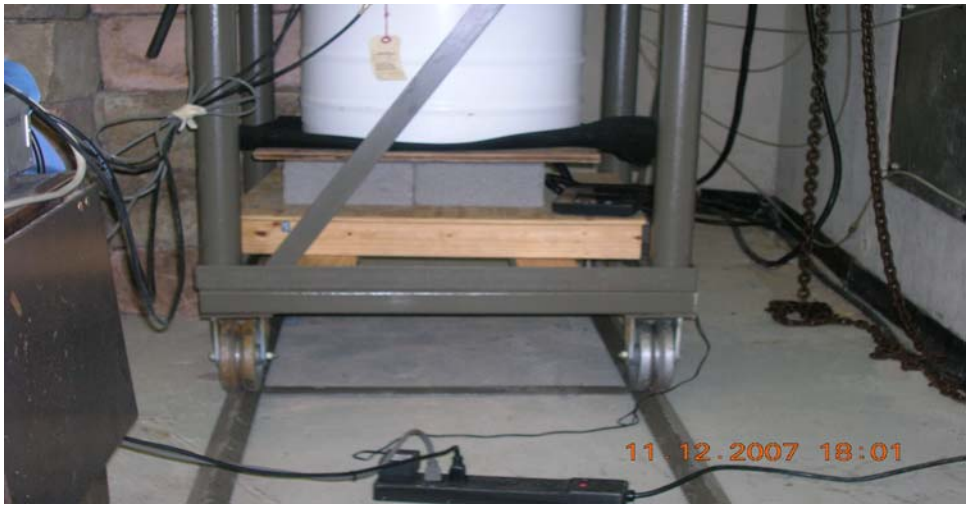

Fig. 3-7. Picture showing HPGe mounted on steel rollers.

The detector is surrounded on all sides by a minimum of 10-cm thick lead bricks. The framework of lead brick shielding being stacked around the detector is as shown in Fig. 3-8. The steel frame raises the detector to the 48-inch height of the beam and the rollers provide variable distance capabilities. The incident gamma radiation from the sample passes through a hole made out of lead bricks to reach the detector. During our investigations, additional shielding was provided around the detector end cap due to high dead time and suspicion of crystal damage to the detector from the germanium peaks observed in the spectra.

Fig 3-8. Picture showing initial shielding around HPGe detector.

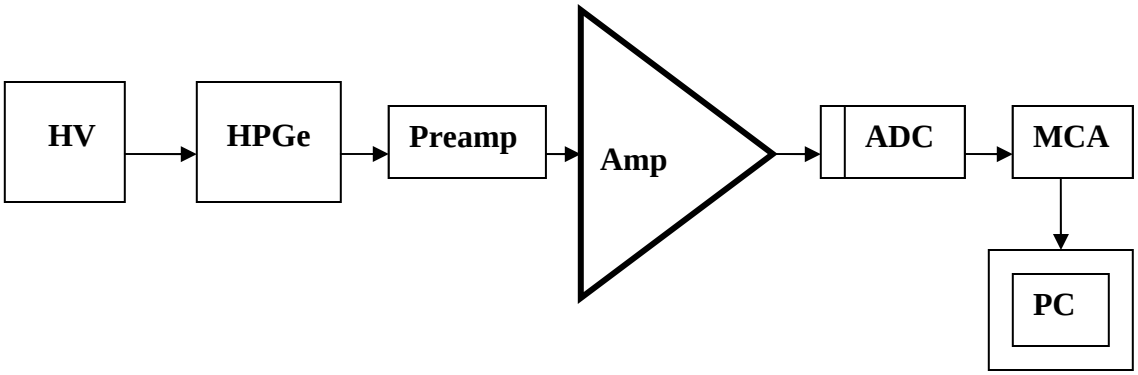

Fig. 3-9. Schematic showing PGNAA detection system and acquisition electronics.

The counting system, illustrated in Fig. 3-9 consists of an Ortec Model spectroscopic amplifier (Ortec 572) and an 8K ADC (ND 575), which was later replaced with a 16K gain ADC (ND581) to accommodate more channels. The ADC processes the signals from the detector, which are collected by an AIM (ND 556) multi-channel analyzer unit controlled by the Canberra Genie 2000 V2.1 Gamma acquisition and analysis software. Other components used were an Ortec Model 441 rate meter, and a Canberra high voltage supply model 3016 D with a 3 KV maximum output. All these components, with the exception of the preamplifier, were housed in a Tennelec NIM BIN (Tennebin 3) retrofitted with an external 6-volt power supply. A Dell Optiplex GX1 brand computer system with Intel Pentium III processor was used. These components were of the low end compared to recent facilities. Specifically, the computer's lower processing speed and the RAM size of 256 MB posed serious limitations during spectral

acquisition. However, we were able to use it for the purpose of demonstrating the principle of PGNAA by reducing the acquisition duration to less than one hour.

DETERMINATION OF SAMPLE POSITION

Real time radiographic images obtained before construction at various horizontal distances from the beam port and vertical heights from the LRL floor were used to determine the ideal location of samples. Although quantitative analysis of image quality and resolution were not done, observations of the real time images as recorded on a DVD, the position having the best image resolution was determined. This position with well resolved images corresponds to that with the most intense beam of neutrons. The ideal position was at 91 cm (36 inches) from the beam port opening along the beam centerline and 1.2 meters (48 inches) height from the LRL floor; other components were built around this position as the sample chamber. Beam divergence was also investigated by obtaining radiographic images at certain angles away from the beam centerline and determined to be minimal. The result of the divergence was useful in our shielding design and detector positioning.

Sample geometry considerations are important for quantitative analysis. While the sample should be positioned at a location with maximum beam fluence, reproducibility of the sample position is also highly desired. During this phase of the project, the neutron radiography camera malfunctioned and the determination of the beam profile at this position using neutron radiography technique widely reported in literature could not be achieved. In its absence, the beam profile at the sample position

was determined by comparing the peak area counts during irradiation of Cd foils at different marked positions in the sample chamber as shown in Table 3-1.

Table 3-1. Peak area counts from cadmium foil at positions in the sample chamber.

Position	Peak area Counts [**Counts per second**]			Detection Dead time (%)	Acquisition Time(secs)
	B-477 keV	**Cd-558 keV**	**H-2223 keV**		
1	4276 [**21.27**]	1267 [**6.30**]	152 [**0.76**]	10.54	201
2	4271 [**21.36**]	1391 [**6.96**]	154 [**0.77**]	10.62	200
3	4333 [**21.67**]	1852 [**9.26**]	157 [**0.79**]	11.2	200

Using the direct correlation between peak area counts and neutron beam intensity, we irradiated cadmium foils of fixed mass on the marked positions on the sample holder. For consistency, we also recorded the peak area counts for H and B peaks. These counts are from neutron capture by shielding materials and substantial variations should not be expected. Since H and B are from the shielding materials, the constancy in counts per seconds in between irradiations is expected. The changes in counts at the Cd peak energy of 558 keV correlates with changes in neutron fluence rate as a function of position. The dram vial used for this investigation is shown in Fig. 3-10.

Fig. 3-10. Dram vials showing markings used to determine sample location.

The maximum peak area counts on the 558 keV line was observed at position #3. This position corresponds to the maximal neutron beam fluence. The dram vial was cut at that mark to serve as sample holder. Cadmium foils were fixed to the side of Teflon vials, attached to the sample holder (cut dram vial) using Kaptan tape and positioned on the sample chamber for irradiation. Fig. 3-11 shows the cut dram vial which was used as sample holder. A new holder was used for each irradiation, to maintain a constant hydrogen background.

Fig. 3-11. Sample holder used for irradiation.

Teflon vials have been widely used as PGNAA sample holders. Teflon vials were obtained from Savillex Corporation and are known to contain lesser amounts of hydrogen than regular poly vials. Lower hydrogen content reduces the background reducing the 2223 keV capture gamma-rays from hydrogen. To maintain a similar geometry, the NaCl sample also used in this investigation was filled in a Teflon vial and attached to the sample holder (cut dram vial) using a Kaptan tape as shown in Fig. 3-12. Kaptan tapes are known to be transparent to neutrons and radiation resistant during irradiation.

Fig. 3-12. NaCl filled Teflon vial attached to sample holder for irradiation.

ENERGY AND EFFICIENCY CALIBRATIONS

After the final set up, energy and efficiency calibrations of the HPGe were carried out in the energy range of 0 to 1407 keV using ^{152}Eu calibration sources. Following this calibration, room background spectra without a sample was acquired without the neutron beam followed by beam background without sample, but with neutron beam. A peak area analysis of the background spectra was generated using the GENIE software. Attempts at irradiating vanadium foil for use in extending the energy calibration up to about 6 MeV were not successful. The small quantity of vanadium available did not produce sufficient activation over two hours to produce measurable peak counts on the HPGe. Calculations predicted the need for a larger mass of vanadium. This will be obtained for this analysis in the future.

SHIELDING CONSIDERATIONS

Shielding around the beam line and the HPGe is important in reducing the neutron and gamma-ray backgrounds to achieve a higher signal-to-noise ratio for the characteristic peaks. At the NSC the detection system is close to the reactor core, hence a high reactor gamma-ray background and scattered neutrons are expected. The issues investigated to determine and improve upon the efficiency of our shielding were the peak counts recorded at the annihilation peak (511 keV), and counts recorded on the germanium peak lines. While the Ge lines provided an indication of neutrons hitting the detector, the annihilation peak gave an indication of inefficient shielding for reactor gamma radiation. Secondary indicators were the net area counts from boron and hydrogen peaks. While preliminary efforts to reduce the counts recorded on these peaks through improvements in shielding materials close to the sample position did not yield remarkable success, more efforts to further reduce these peaks are being investigated and will be given adequate attention during the next phase of the project. Facilities reviewed have used highly enriched Li-6-based shielding materials in the form of ^{6}Li loaded polymer to shield the detector from scattered neutrons. Li-6 completely absorbs neutrons without emission of capture or decay gamma-rays using the reaction ^{6}Li (n,α) ^{3}H.

An overhead view of the complete facility is shown in Fig. 3-13.

Fig. 3-13. Aerial view of PGNAA facility at NSC.

PGNAA ANALYSIS

To investigate the detection capability of our PGNAA system, known masses of cadmium foils and NaCl sample were irradiated for about 2000 seconds and the results compared with our theoretical predictions. Irradiation durations were limited to about 2000 seconds partly because of the processing speed of the computer system. Also, the NSC is a multi-user facility, and one of the design objectives was to investigate the feasibility of providing the PGNAA analysis within shorter duration with increased sample mass.

For each spectrum, the peak analysis was generated using the Genie acquisition and analysis software. The peak area counts recorded for the gamma energies for each of the sample investigated were compared with the results of our theoretical predictions. The most intense gamma-ray energies of Cl and Cd were used for our analysis. A prompt gamma-ray spectrum catalog has been developed (Revay et al. 2004) based on measurements in various experimental facilities that provide information on the gamma-ray energies for elements and isotopic components. The database was developed as part of the Coordinated Project for the Development of a Database for Prompt Gamma-ray Neutron Activation Analysis sponsored by the International Atomic Energy Agency (IAEA 2003) to improve the accuracy and completeness of the data needed in the technique of prompt-gamma activation analysis. The database provides additional information such as the thermal neutron capture cross sections (partial and total), isotopic composition, Westcott g-factors, decay mode, half life and branching ratios, etc.

PREDICTIVE MODEL

The experimentally measured net peak area count rate for a particular gamma-ray line in the spectrum can be predicted using Eqn. (2.8)

$$C = \frac{mN_a}{M}\Phi\varepsilon(E_\gamma) f\sigma P_\gamma = \frac{mN_a}{M_a}\Phi\varepsilon(E_\gamma)\sigma_\gamma \qquad (2.8)$$

The net peak area counts over the duration of irradiation can be obtained simply by multiplying Eqn. 2.8 by the acquisition time in seconds. The average thermal neutron fluence rate interacting with the sample was measured experimentally to be 9.3 $X10^5$ n cm^{-2} s^{-1} and this is assumed to remain constant. The gamma rays of a particular energy are detected with absolute detector efficiency measured using the NIST standard calibration source. For any gamma-ray energy, the absolute detection efficiency is calculated using the efficiency equation from GENIE

$$\ln[\varepsilon(E\gamma)] = 188.514 - 206.590 \ln(E\gamma) + 83.122 \ln(E\gamma)^2 - 16.125 \ln(E\gamma)^3 + 1.517\ln(E\gamma)^4 - 0.056 \ln(E\gamma)^5 \qquad (3.1)$$

The partial gamma-ray production cross sections, is the product of the emission probability of the gamma-ray and the isotopic capture cross section as well as the natural abundance of the isotope in the element. These values, which give the number of photons that will be emitted from the element during irradiation, are given in the database of PGNAA. The number of photons that will be detected per gamma ray line is a function of the counting efficiency of the system. Using these values, we can optimize

the net peak area counts by a combination of irradiation duration and by careful selection the mass of the element, which will give the number of atoms available for interaction with the neutrons. An extract from the PGAA Prompt Gamma Data (IAEA 2003) for the 788 keV and 1164 keV energy lines of ^{36}Cl is shown in Table 3-2.

Table 3-2. Extractions from the PGAA prompt gamma data showing partial gamma-ray production cross sections for ^{36}Cl. (PGAA Prompt Gamma Data [database online] IAEA ,2003).

Isotope	E(γ) keV	σ_γ(barns)	Uncertainty
^{36}Cl	788.428	5.4	0.05
^{36}Cl	1164.87	8.9	0.04

Using Eqn (3.1), the efficiency of the gamma-ray lines are calculated as 8.0×10^{-5} and 6.3×10^{-5} respectively. To obtain a measurable net peak area counts, 6.37 grams of NaCl was obtained. The relative concentration of chlorine in the sample is about 60.66% which gives 3.8669 grams of chlorine. The number of atoms in 3.8 grams of chlorine was calculated to be 6.468×10^{22} atoms using the equation:

$$n = mN_A/M \qquad (3.2)$$

where:

n = number of atoms in 3.8 grams of chlorine

m = mass of chlorine;

N_A = Avogadro's number; and,

M = relative atomic mass of chorine

Substituting for all other values in Eqn. (2.8), we expect to record 26.1 and 33.8 counts per seconds respectively with about 52,200 and 67,500 net peak area counts expected over 2,000 seconds respectively. The model serves as a guide to optimizing the net peak area counts using the duration of irradiation and masses of samples. For our studies, it served to predict the net peak area counts for comparison with experimental results and hence evaluation of the performance capability of our facility. Experimental results and comparison with calculations using the predictive model are presented in the next chapter.

CHAPTER IV

RESULTS AND DISCUSSIONS

The results of a series of investigations into the problems with developing a PGNAA system at the Nuclear Science Center of Texas A&M University are presented. Beam characterization and the efficiency of the HPGe used to measure prompt gamma-ray energies are reported. Spectral analysis of results from irradiation of 0.64 grams of Cd foil and 6.37 grams of NaCl is presented. Based on the theoretical model developed, the count rates predicted for the most intense peaks in given masses of cadmium and chlorine under given experimental conditions are presented and these results are compared with experimental yields of prompt gamma-rays from these samples as measured.

BEAM CHARACTERISTICS

After some modifications, the neutron beam used for this experiment was filtered using a sapphire crystal placed in the graphite plug towards the core end of the beam port. The average thermal neutron fluence rate that was measured recently at the sample location was 9.3×10^5 n cm^{-2} s^{-1}, with an average epithermal fluence rate of 4.58×10^2 n cm^{-2} s^{-1}. The modifications has improved the cadmium ratio from 5.57 to about 122 at the sample position, but with a reduction of beam fluence rate from 8.758×10^6 n cm^{-2} s^{-1} to 9.3×10^5 n cm^{-2} s^{-1} as expected. The higher cadmium ratio is actually due to the lowering of epithermal component in the beam.

The collimator presently in use has reduced the beam divergence around the beam port opening in the Lower Research Level. The images taken with a radiographic camera showed a better collimated beam outside of BP #1 opening. An example of a collimated image taken is shown in Fig. 4-1.

Fig 4-1. Radiography image of neutron beam at BP# 1 opening.

The sample position was determined using beam port radiographic mapping as described in the previous chapter. Samples are irradiated in air at a distance of about 92 cm (36 inches) from the beam port opening and approximately 1.22 meters (48 inches) above the LRL floor with a sample to detector distance of about 55 cm (21.5 inches). This distance can be varied, down to a minimum of about 38 cm (15 inches).

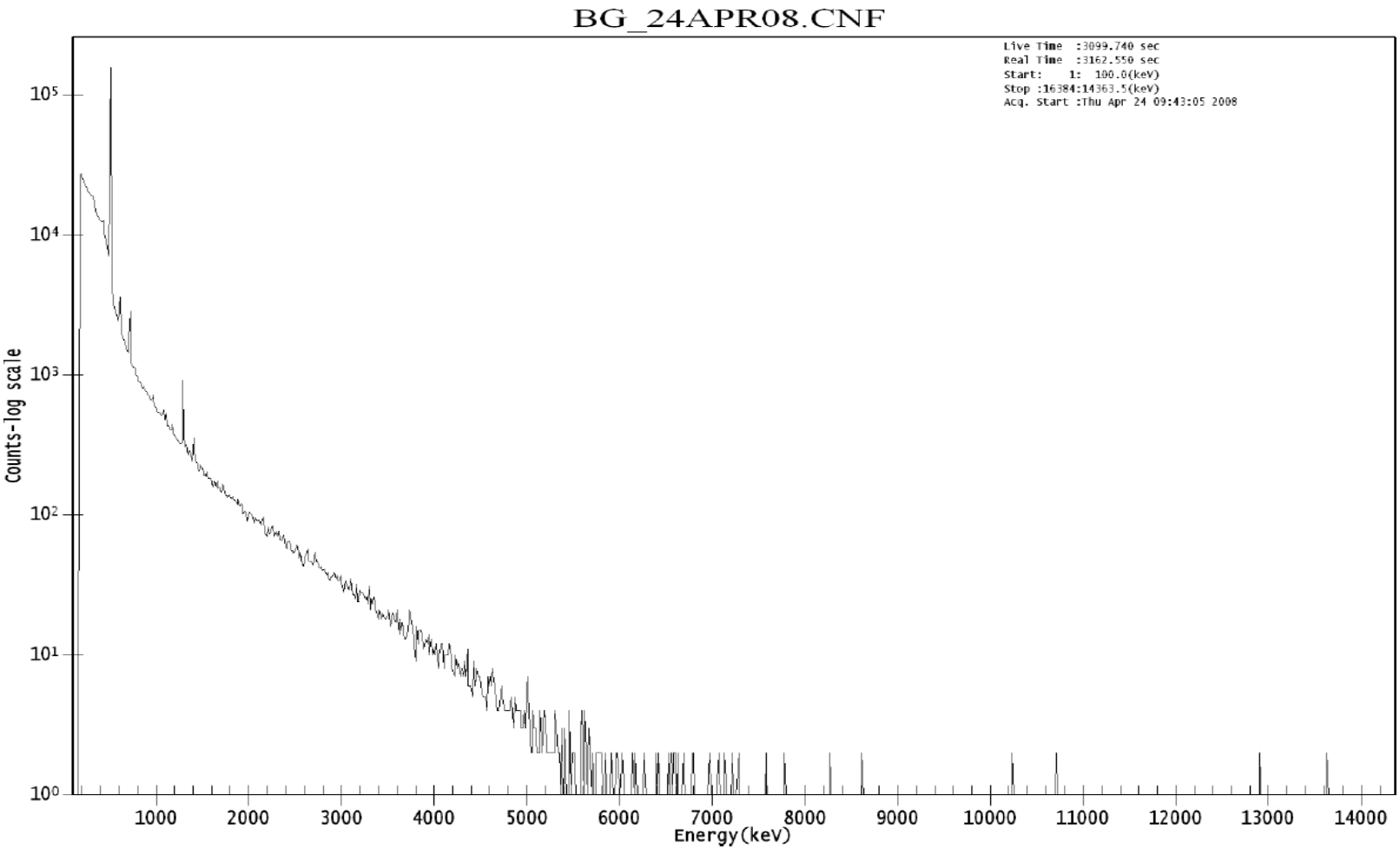

Fig. 4-2. Room background spectrum for 3099.7 seconds without neutron beam.

detector was placed at 90° with respect to the neutron beam direction. The replacement of the 8K ADC with the 16K gain ADC (ND581 model) improved the detector energy gain to approximately 1 keV per channel covering about 165 keV to over 12 MeV.

The room background spectrum acquired for about 3000 seconds at full reactor power without neutron beam i.e. the water shutter closed is shown in Fig. 4-1. All the peaks in the spectrum from the peak search were within 0 to 2000 keV. The peak searches were performed on these spectra utilizing the Canberra GENIE 2000 peak analysis routine and the results of peak searches may be found in Appendix A-1. The peak locate threshold of 3.00 which incorporates the second differential peak search routine for unidentified peaks was utilized. Energy tolerance of 1.0 keV was used to match the peaks. Most of the peaks identified were within 1.0 keV of the library values. For regions greater that 1.4 MeV, the uncertainty in the energy calibration is higher due to large spacing between the calibration points. For example, the prompt peaks of hydrogen (2223 keV) was located around 2225 keV. Identification of the peaks generated from GENIE acquisition software for the room background spectrum is displayed in Table 4-1. Contribution to the room background is mainly from the annihilation peak at 510.86 keV. The 182.07 keV peak could not be identified and is possibly an artifact of the cutoff by the lower level discriminator. Decay gamma-ray from ^{41}Ar at 1294.27 keV produced by neutron activation of air is observed. Air has ^{40}Ar as a natural constituent and the modest cross-section of ^{40}Ar for thermal neutron activation makes production of ^{41}Ar technically difficult to eliminate particularly for low flux reactors like the NSC's TRIGA reactor. The 614.04 and 722 keV peaks are decay gamma-ray emissions either from germanium

crystal in the detector which is evidence of neutrons interactions. Overall, a high Compton continuum is evident from the reactor gamma radiation.

Table 4-1. Peak identification in room background spectrum from Fig. 4-2.

Energy (keV)	Net peak Area	Counts per second	Identification
182.07	1.04 E+005	33.6	Background unknown
433.95	5.96 E+003	1.9	^{108}Ag metastable?
510.86	7.60 E+005	245.2	511 keV annihilation peak
614.04	6.64 E+003	2.1	^{77}Ge decay peak
722.58	7.29 E+003	2.4	^{79}Ge decay peak
1294.27	3.49 E+003	1.1	^{41}Ar peak

Fig. 4-3 shows the beam background spectrum acquired at the full reactor power of 1.0 MW with the neutron beam turned on by opening the water shutter with an empty sample chamber for 3602 seconds. The peak area counts of the beam background generated with GENIE code is shown in Appendix A-2. Contributions in beam background have been identified by Revay et al. (2004) to include natural background, low energy x-rays, activation products, prompt gamma-rays from the (n,γ) reaction. Also identified are the (n, 2nγ), (n, n′γ) and annihilation gamma-rays.

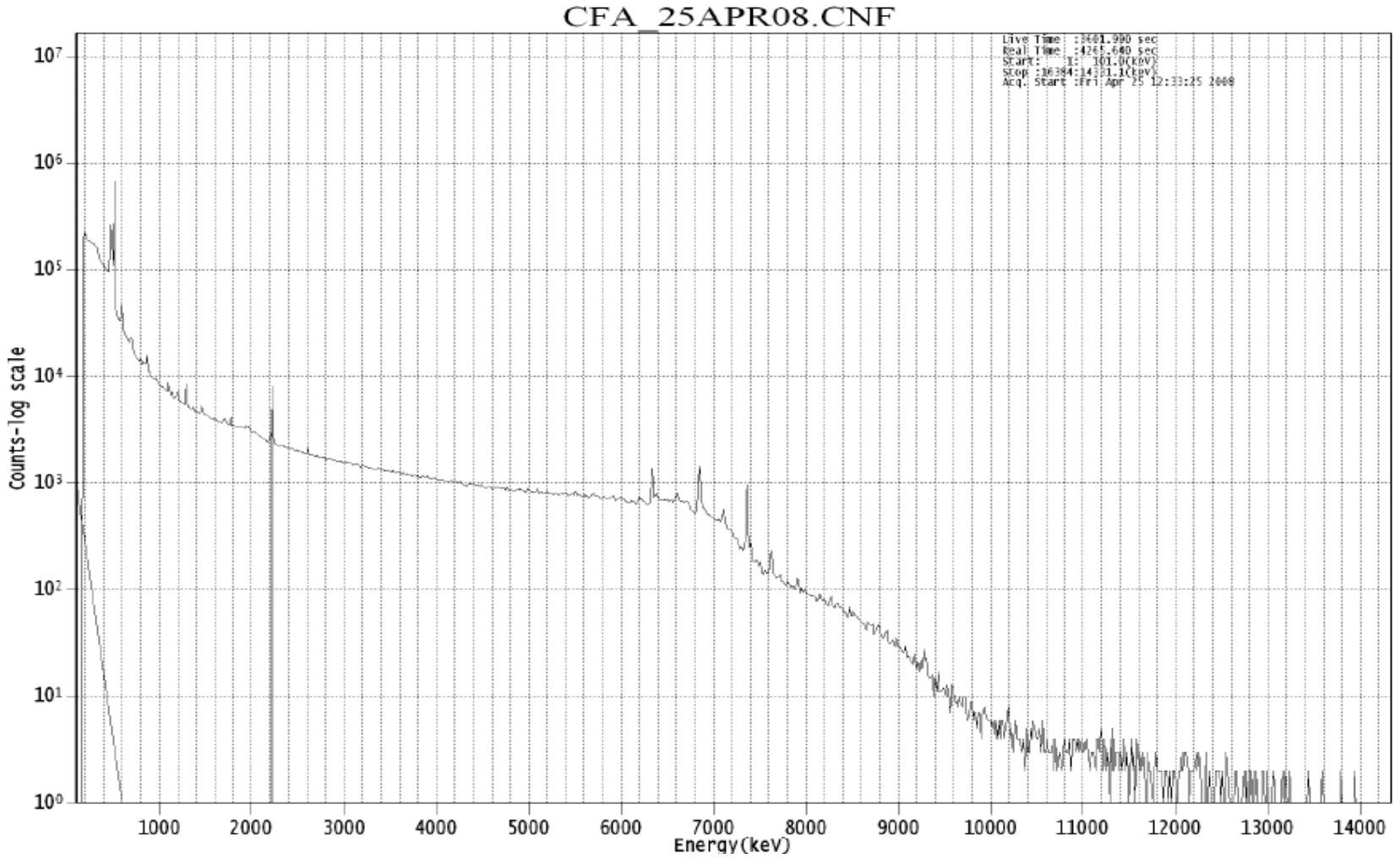

Fig. 4-3. PGNAA background spectrum with neutron beam acquired for 3602.0 seconds.

An attempt to identify the peaks in the beam background is shown in Appendix A-3. Apart from the annihilation peak and the 182 keV peak, the 477.14 keV prompt peak from boron is very prominent with about 500 cps. Prompt peaks of hydrogen at 2221.68 keV with about 14 cps. Boron and hydrogen prompt peaks originate from the borated polyethylene material used for neutron shielding along the beam collimator. Low energy x-rays from lead and activation products of the germanium crystal in the detector are also seen in the peak analysis as well as the 1778 keV decay peak from aluminum activation. Germanium peaks originate from the HPGe crystal and it is an indication that stray neutrons are hitting the detector, evidence of inadequate shielding for neutrons. Contribution from Al could have originated either from the BP #1 collimator or the aluminum material housing the germanium crystal in the detector, but this could not be confirmed with certainty.

EFFICIENCY MEASUREMENT WITH ^{152}EU POINT SOURCE

The counting efficiency of the detection system was determined using a standard calibration ^{152}Eu point source from the National Institute of Standards and Technology (NIST). The certificate of calibration for this source is shown in Appendix B. The point source spectrum was acquired for about 18000 seconds and the plot of absolute detector efficiency against energy is shown in Fig. 4-4.

Eqn 3.1 is the best fit line given in the fifth order polynomial.

$$\ln[\varepsilon(E\gamma)] = 188.514 - 206.590 \ln(E\gamma) + 83.122 \ln(E\gamma)^2 - 16.125 \ln(E\gamma)^3 + 1.517\ln(E\gamma)^4 - 0.056 \ln(E\gamma)^5 \quad (3.1)$$

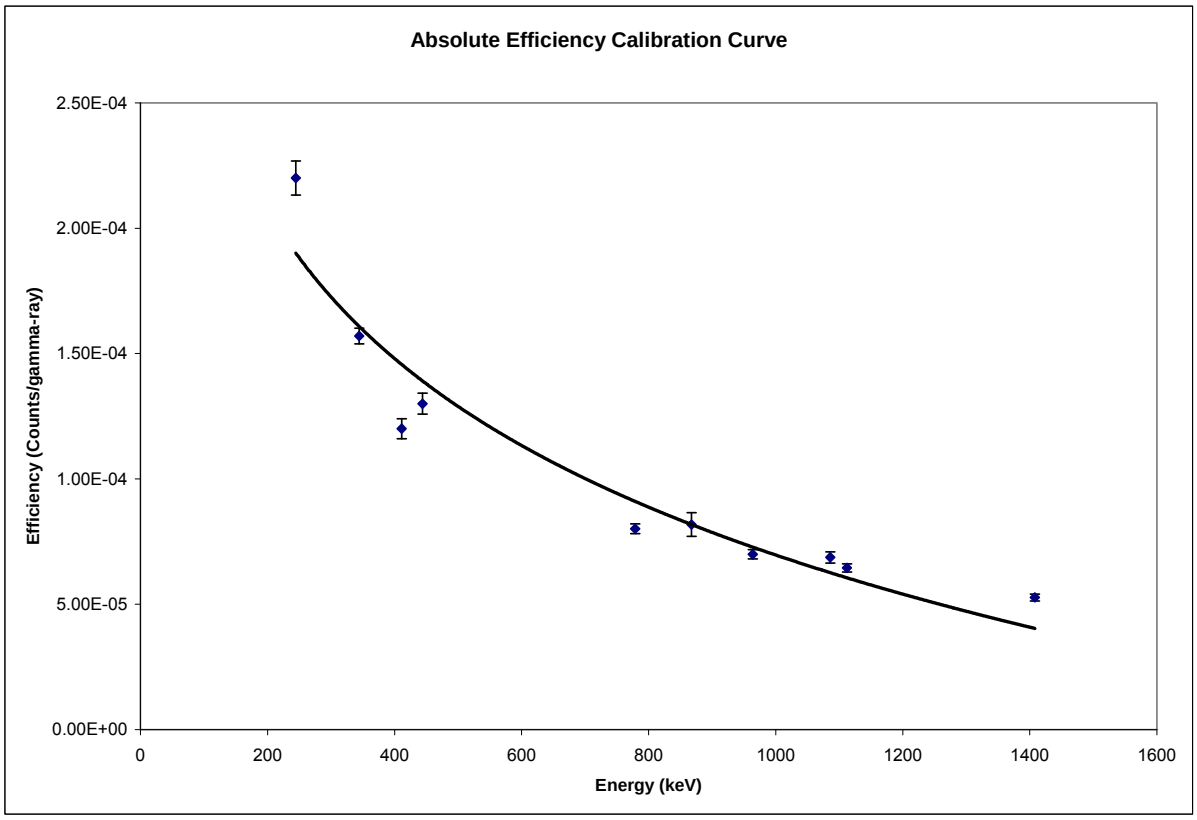

Fig. 4-4. Absolute detector efficiency vs. energy for ^{152}Eu.

SAMPLE DESCRIPTIONS

Elements used in this study were chlorine and cadmium, obviously because of their large thermal neutron cross sections and ease of analysis. Also, many of the very intense prompt gamma lines as well as the recommended gamma-ray lines used for analytical

sensitivity calculations for these elements are within the range of ^{152}Eu calibration energies. The recommended energy line of cadmium is 558 keV while those of chlorine are 786 keV and 788 keV. The absolute efficiency for these gamma-ray lines was determined using our NIST calibration source. Cadmium was available as pure foils while chlorine in the form of NaCl standard, CAS # 7647-14-5 with 99.9% purity was obtained from the NSC. Using the standard 60.66% of chlorine by weight of NaCl compound, 6.37 grams of NaCl standard used gave about 3.8669 grams of chlorine element. The number of chlorine atoms in 3.8669 grams was calculated using the Eqn (3.2). This gives about 6.4686 x 10^{22} atoms of chlorine. Similarly, the number of atoms in 0.64 grams of cadmium foil used is 3.54 x 10^{20} atoms. The nuclear reactions of interest for chlorine and cadmium are the (n,γ) reaction. Only one principal isotope is produced per sample and this is due to the percentage abundance and differences in their partial cross sections. Naturally occurring cadmium element has about 12.22 % of ^{113}Cd isotope with thermal neutron cross section of 20600 barns and chlorine element has about 75% of the isotope ^{35}Cl with thermal neutron cross section of 43.6 barns. These two elements used are very amenable to neutron capture reactions.

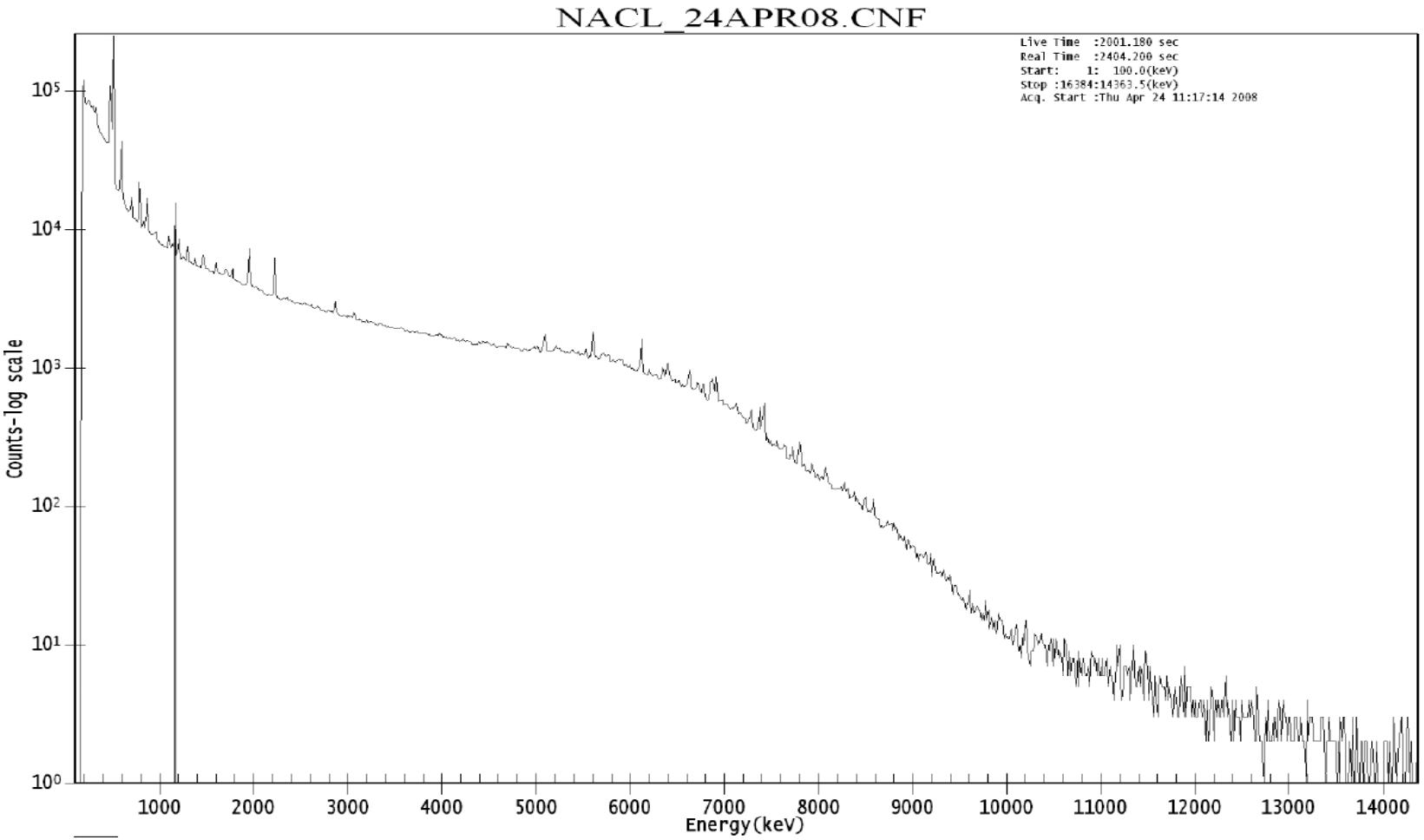

Fig. 4-5. Chlorine prompt gamma-ray spectrum. The spectrum was acquired for a live time of 2001.2 seconds.

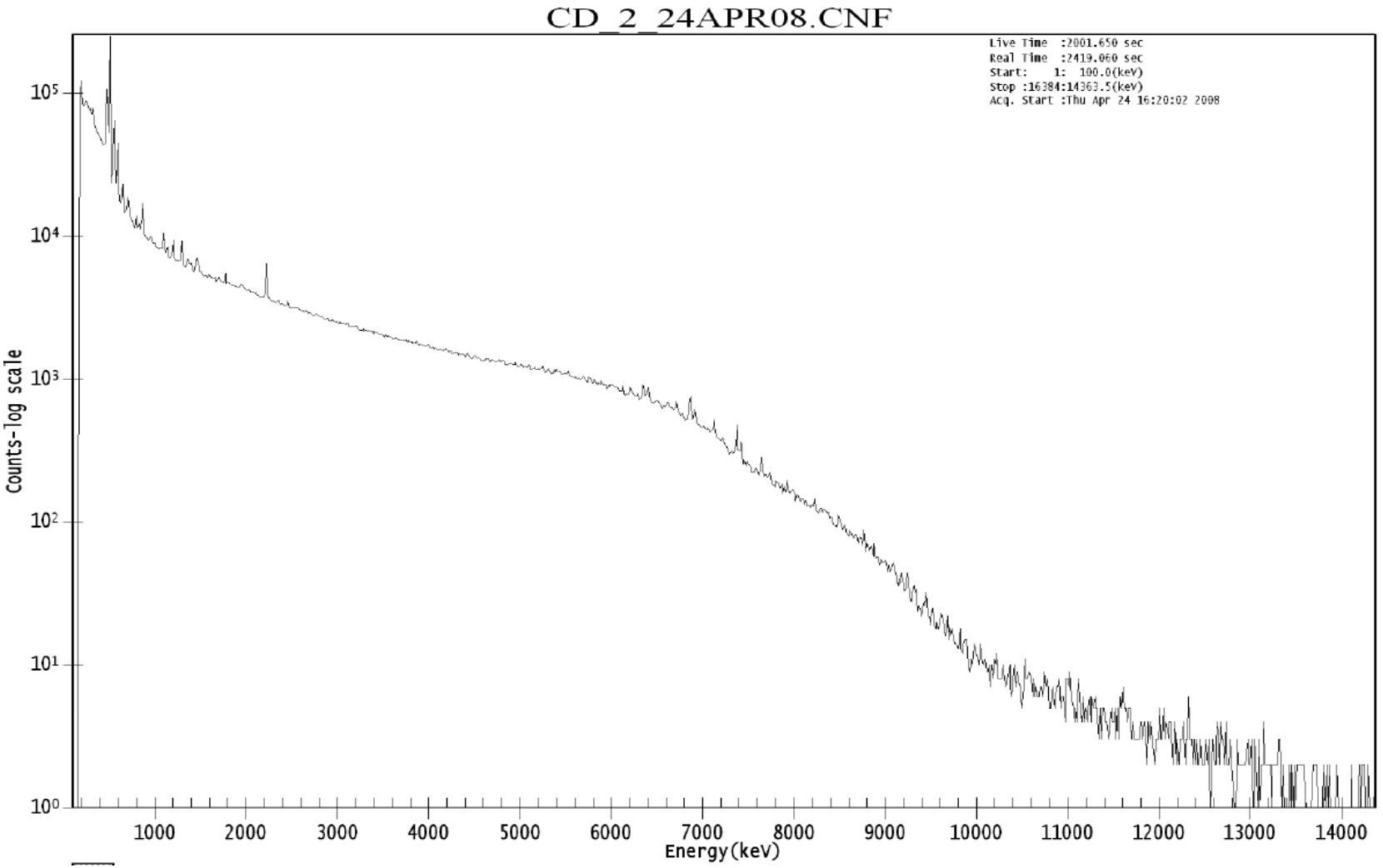

Fig. 4-6. Cadmium prompt gamma-ray spectrum. The spectrum was acquired for a live time of 2001.6 seconds.

CHLORINE AND CADMIUM MEASUREMENTS

Samples were irradiated separately and the gamma spectra for chlorine and cadmium were acquired for about 2000 seconds each using the NSC's PGNAA experimental facility. The prompt gamma spectrum of cadmium and chlorine is shown in Figs. 4-5 and 4-6 respectively. Peak searches on the spectra of chlorine and cadmium can be found in Appendix C. Utilizing the measured detector efficiency from ^{152}Eu data, the neutron beam fluence rate, and the individual sample data, the prompt gamma-ray yield i.e. net peak area counts for the most intense prompt gamma-ray energies was calculated using equation (2.8) for chlorine and cadmium. Prompt-gamma energies, mainly in the range of calibration source gamma-ray energies (0-1407 keV) were considered in this investigation. The energy dependent efficiency ε ($E\gamma$) is calculated for each gamma-ray line using the absolute detection efficiency Eqn 4.1 which is valid for energies up to 1407 keV. The table of calculated efficiencies for the most intense peak energies of Cd and Cl considered in this analysis is shown in Appendix D. Attempts to measure the prompt gamma-ray detection efficiencies for higher energies using vanadium sample was unsuccessful and is discussed later. The actual detection efficiencies for the 1601.07 keV, 1951.14 keV and the 1959.35 keV lines of chlorine will be slightly higher than our estimation using the detection efficiency equation of ^{152}Eu because these efficiencies are extrapolated beyond our calibration energies. The estimate of the efficiencies at these energies will slightly underestimate the peak area counts in this analysis, but this is sufficient for demonstration purposes.

The net peak area counts for each gamma-ray peak is given by

$$C_\gamma = \varepsilon(E_\gamma) n \sigma_\gamma \Phi \qquad (2.8)$$

where:

n= the number of atoms is given as

$$n = \frac{mN_A}{M} \qquad (3.2)$$

As an example of the above calculation, the peak area counts of the 558 keV prompt gamma line of cadmium with detection efficiency of 1 x 10^{-4} counts per gamma-ray is given below:

$$C_\gamma = 1\times10^{-4} \times 2000s \times \frac{0.64 grams \times 6.022\times10^{23}}{113} 1860 barns \times 9.3\times10^{5}\, ncm^{-2}s^{-1}$$

$$= 1.18 \text{ x } 10^6 \text{ counts.}$$

For our calculations, we have assumed a constant flux of neutrons at the sample and a constant number density over the volume of the sample. The gamma-ray energy peaks within each spectrum were identified by manually inspecting the peak area analysis generated from the GENIE software. The uncertainty in experimental values of the peak area counts were obtained from the net area uncertainty in the peak analysis report generated from the GENIE analysis software. Results of net peak area calculations can be found in Appendix E.

The net peak area count of the energy lines of the prompt gamma-ray of chlorine is shown in Table 4-2. Prompt gamma-ray peaks of chlorine at 517, 786 and 1162 keV had no counts and were not identified in the spectrum peak search.

Table 4-2. Peak area counts of prompt-gamma-ray for chlorine.

Calculations		**Experimental**			**Isotope**	**Difference (%)**
Energy (keV)	**Peak area Counts**	**Energy (keV)**	**Peak area Counts**	**Uncertainty (±)**		
*517.07	9.72 x 10^4	517.07*	0*	N/A	^{36}Cl	N/A
*786.30	3.30 x 10^4	786.30*	0*	N/A	^{36}Cl	N/A
788.43	5.22 x 10^4	787.58	7.62 x 10^4	847.07	^{36}Cl	-46.02
1131.25	4.85 x 10^3	1131.64	5.75 x 10^3	244.81	^{36}Cl	-18.60
*1162.74	5.77 x 10^3	1162.74*	0*	N/A	^{36}Cl	N/A
1164.87	6.75 x 10^4	1165.31	6.13 x 10^4	729.48	^{36}Cl	9.22
***1601.07*	***6.45* x 10^3**	***1602.06*	***7.50* x 10^3**	***562.72*	**^{36}Cl**	***-16.28***
***1951.14*	***2.25* x 10^4**	***1953.40*	***2.55* x 10^4**	***263.00*	**^{36}Cl**	***-13.42***
***1959.35*	***1.44* x 10^4**	***1961.89*	***1.68* x 10^4**	***247.26*	**^{36}Cl**	***-16.63***

* Energy line not found in experimental spectrum

N/A--- No results available.

** *Results are not accurate. Efficiencies are based on estimates, not measured.*

Apart from of the 517 keV energy line which was not be detected due to the high Compton continuum around the 511 keV annihilation peak, the partial capture cross sections of the other two peaks are smaller, compared to the others that were detected in the spectrum. Three peaks were located in the region of 0 to 1407 keV. Overall, a comparison of the predicted and experimentally measured values of net peak area counts for energies of chlorine show a good agreement. With the exception of the 1164 keV

line, more net peak area counts were measured than predicted using our model (Fig. 4-7).

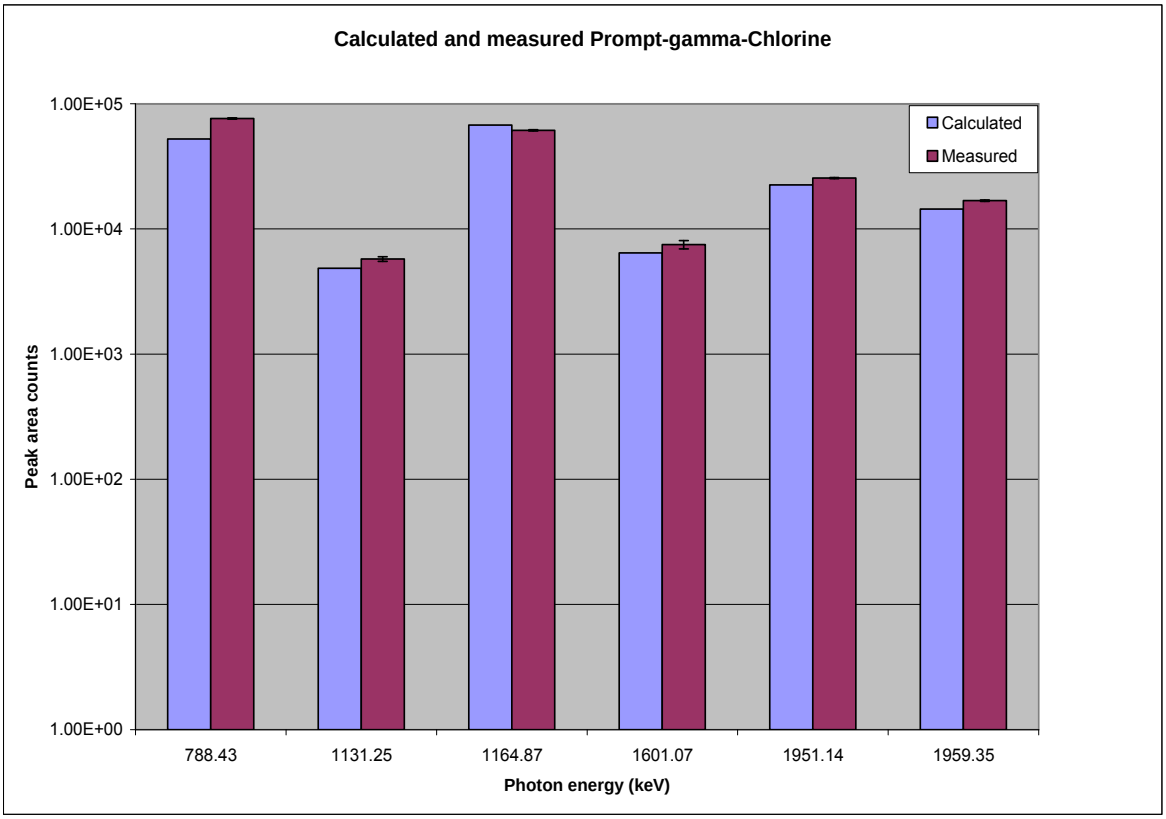

Fig 4-7. Calculated and experimentally measured peak area counts for the most intense prompt-gamma-ray energies of chlorine.

The differences between predicted and experimental values for chlorine can be attributed to many factors. We had assumed a constant thermal neutron fluence rate interacting with the sample throughout the duration of irradiation, but in practical terms,

variations in neutron fluence rate may not be negligible. The net peak count rates for boron and hydrogen is expected to remain constant in between irradiation. However, during irradiation of cadmium, the peak count rate for boron and hydrogen were 338 and 13 respectively but during irradiation of chlorine, count rates of 354 and 13 were observed. The higher count rate on boron peak indicates some variation in beam fluence which could contribute to some errors in our predicted net peak area counts. The use beam flux monitors and recommended normalization techniques were not incorporated in this phase of our investigations. There are uncertainties associated with the beam fluence rate measurements, absolute efficiencies and partial gamma ray cross section data which were not accounted for in our calculations.

A large mass of NaCl was irradiated and the effects of self-shielding and gamma self absorption are possible. We cannot also assume uniformity and homogeneity of the sample. The Teflon vial was filled with the NaCl sample, and there could be some air spaces in between the crystals which will introduce non uniformity as opposed to a uniform solid mass of metal. The mass of the sample could also result in attenuation of the prompt-gamma rays, which was ignored in our calculations. While it is pertinent to note that the detection efficiencies for the 1601.07, 1951.14 and the 1959.35 keV lines of chlorine were slightly underestimated, the predicted results are in agreement with the observed trend. The determination of absolute efficiencies above 1407 keV will be required to further confirm these results.

The experimental and predicted net peak area count of the most intense prompt gamma-ray energies of cadmium is shown in Table 4-3. Results obtained from

irradiation of cadmium show much difference between the predicted and experimentally measured values. Overall, as shown in Fig. 4-8, more counts were predicted through our model than measured experimentally.

Table 4-3. Peak area counts of prompt-gamma-ray for cadmium

Calculations		Experimental			Isotope	Difference (%)
Energy (keV)	Peak area Counts	Energy (keV)	Peak area Counts	Uncertainty (±)		
558.32	1.18 x10^6	558.32	2.35 x10^5	6.33 x10^2	^{114}Cd	80.15
651.19	2.04 x10^5	651.17	4.71 x10^4	9.79 x10^2	^{114}Cd	76.95
805.85	6.72 x10^4	805.90	1.94 x10^4	3.47 x10^2	^{114}Cd	71.12
1209.65	4.73 x10^4	1210.61	8.34 x10^3	5.12 x10^2	^{114}Cd	82.37
1364.30	4.26 x10^4	1365.30	7.63 x10^3	2.45 x10^2	^{114}Cd	82.10
1399.54	3.29 x10^4	1400.42	5.87 x10^3	2.44 x10^2	^{114}Cd	82.17

This is different from chlorine and the discrepancies are very large. The observed differences are as expected for cadmium due to its large cross section with a consequent large effect of self-shielding. For typical surface densities of foils, the self-shielding effects are of importance for cross sections greater than 10 barns. The effect can be measured using the self-shielding coefficient, which is the self shielding factor describing the flux perturbation due to the existence of neutron absorption within the foil. The coefficient which varies between 0 and 1 depends on the product of macroscopic absorption cross section and foil thickness for a given neutron energy. It also has been found to depend on the type of incident neutron field, whether isotropic or parallel beam. The self shielding effect refers to the modification of the neutron field

within the foil, but from the point of view of reaction rates, it does not matter whether the modification is on the neutron fluence rate or the cross section.

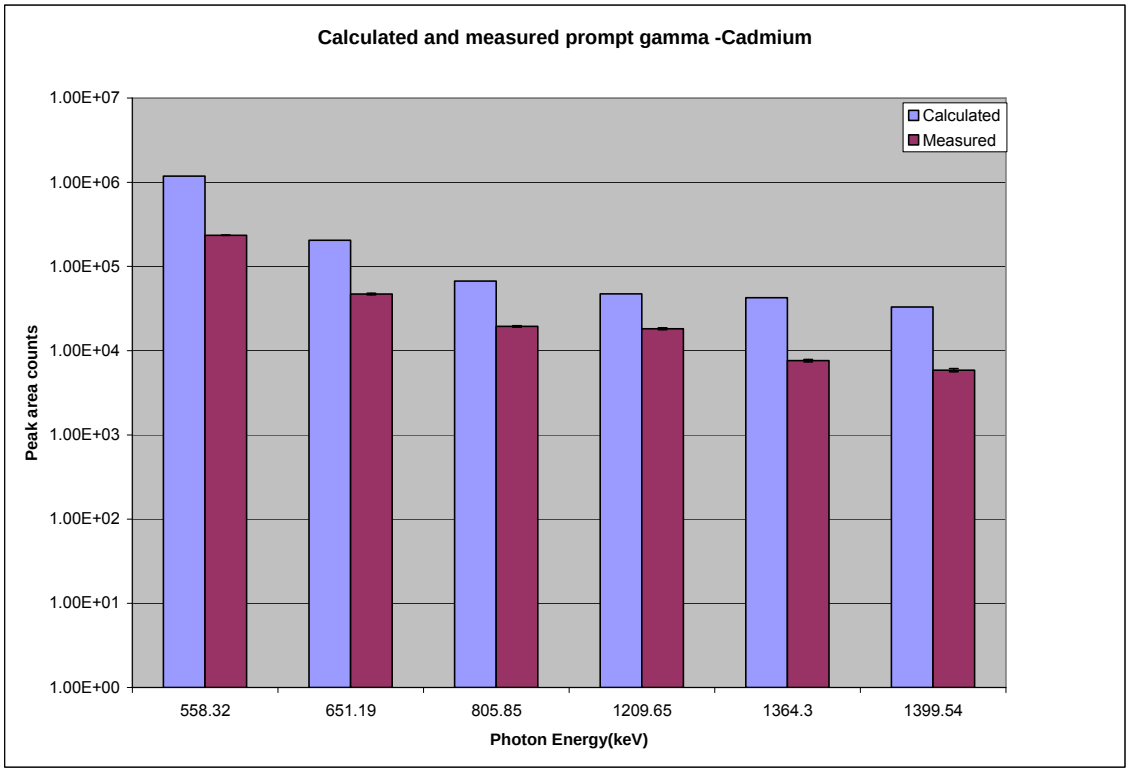

Fig 4-8. Calculated and experimentally measured peak area counts for the most intense prompt-gamma-ray energies of cadmium.

Since cadmium is a known strong neutron absorber, the effect of neutron shielding by cadmium foils was investigated in an attempt to explain the discrepancies observed between the predicted and experimental results. When absorbers like cadmium

of thickness 0.058 cm is placed in a collimated beam of neutrons like the PGNAA irradiation facility, the transmitted neutron intensity, and hence the reaction rate is decreased exponentially as a function of the macroscopic cross section and thickness thus:

$$RR = N\sigma_{\gamma}\Phi \int_{0}^{0.058cm} e^{-\Sigma x}\, dx \qquad (4.1)$$

where:

RR = the reaction rate per second;

N = the number of absorber atoms per unit volume [atoms-cm^{-3}];

x = the foil thickness =0.058 cm; and

$\sum$ = the macroscopic cross section which is defined as the product of the atomic density of cadmium N and the microscopic cross section σ.

σ_{γ} and Φ are as earlier defined.

Evaluating the integral gives the reaction rate as

$$RR = \frac{N\sigma_{\gamma}\Phi}{\Sigma}$$

and Σ =116.64 cm^{-1}

The foil is places at 45 degrees with respect to the beam axis and this introduces a loss factor of 1/1.414 to the neutron fluence component incident on the cross sectional area of the foil. For a complete evaluation of the self-shielding effect, we use the relation

$$RR = \frac{\Phi_0}{\sqrt{2}} \times \varepsilon(E_\gamma) \times N \times \frac{\sigma_\gamma(E_\gamma)}{\Sigma} \times A \qquad (4.2)$$

where:

A = the cross sectional area of 1.28 cm^2 determined by the ratio of foil volume to thickness.

Using the density of cadmium 8.65 g cm^{-3} and the mass of foil used, the value of N = 4.61 x 10^{22} atoms cm^{-3} was determined. Eqn. (4.2) was used to re calculate the predicted net peak area counts over the irradiation period for cadmium incorporating the effects of self shielding and the results are shown in Appendix E-4. The results show that the effective thermal neutron fluence interacting with the foil was reduced or a factor of 9.5 as a result of self-shielding effect. With corrections for self- shielding applied to our predictive model, the observed discrepancies were reduced as shown in Fig 4-9. More net peak area counts is measured than predicted and this is the trend observed for chlorine.

Other sources of errors can be attributed to losses from scattered neutrons which do not interact with the foil, but on shielding materials. Under ideal conditions, the sample should be interacting with all the neutrons as assumed in the calculations, but in practice, not all the neutrons interact with the sample. As evident in our PGNAA background spectrum, neutrons from the source have found their way to interact with shielding materials and the HPGe detector. The attenuation of prompt gamma-rays

which are emitted in the sample matrix from reaching the detector is another source of error and may not be negligible after all.

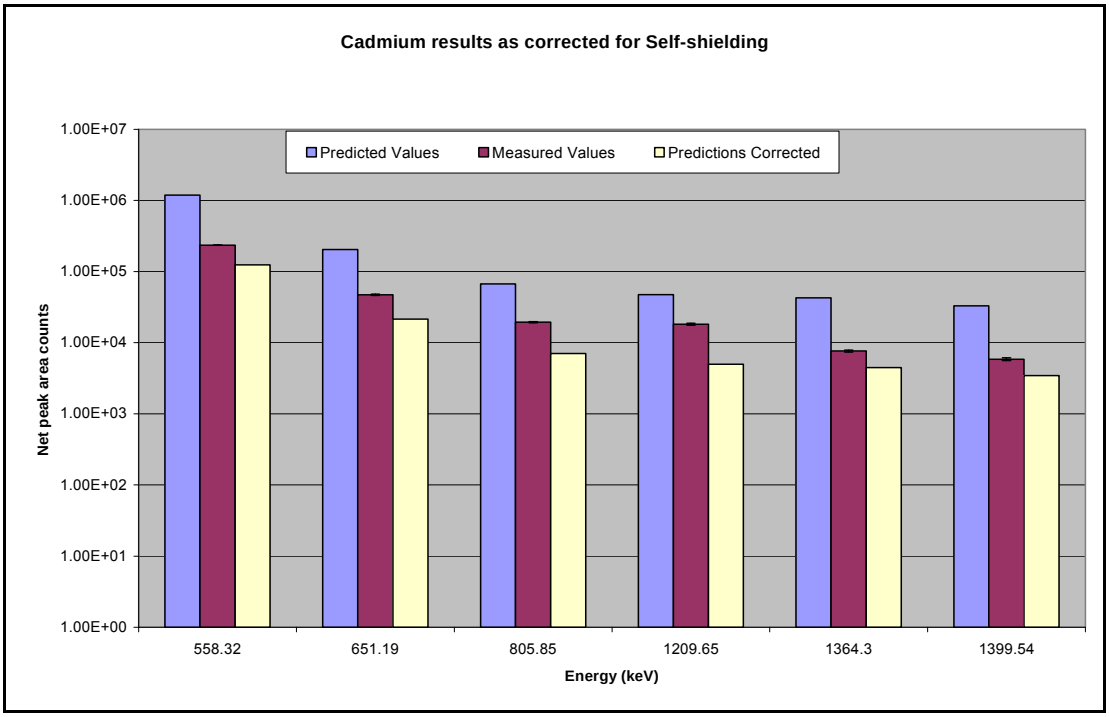

Fig. 4-9. Calculated and measured peak area counts for the most intense prompt-gamma-ray peaks of cadmium as corrected for self shielding.

We have assumed that the beam is a collimated neutron beam, but this may not hold true. Against the assumption of a homogenous sample in our calculations, the sample may not be thin enough to be considered fairly homogeneous to neglect the effects of neutron field attenuation by the sample. We have assumed negligible edge effects. Another typical issue would be the variation of neutron fluence during irradiation. We

did assume constant beam fluence for our calculations, but in practice, this is not so from irradiation to irradiation.

DISCUSSION

The most intense characteristic peaks were identified in the spectrum of cadmium and chlorine. While the experimental results for cadmium were less that predicted values, the opposite was observed for chlorine. However, the results for chlorine and cadmium were statistically significant. Further investigations will be required to reduce the errors. As expected of peaks in the PGNAA spectrum, various peaks were observed in the spectrum which includes peaks from sources other than the prompt gamma-rays from the sample under investigation like the room background, the PGNAA background which originates from neutron interactions in air and the shielding materials. Other sources would include delayed gamma radiation from the shielding materials. Also, gamma-rays with energies above 1.022 MeV have the probability of undergoing annihilation interaction. The single and double escape peaks resulting from the annihilation interaction between gamma energies above 1.022 MeV and the detector were observed in the spectrum.

Vanadium irradiation

A vanadium foil (mass 0.14 grams) was irradiated for about 2000 seconds. We intended to use the decay 1.4 MeV peak along with prompt gamma peaks around 6 MeV to extend the efficiency calibrations to the high energies. However, no peaks were observed

in the spectrum. The detection efficiency of the 1434 keV peak would not differ significantly from the 1407 keV peak of ^{152}Eu. Using the efficiency of the 1407 keV energy line of ^{152}Eu, the number of counts predicted through calculations at the 1434 keV of vanadium during that duration of irradiation would be about 762 counts. Given the Compton continuum of about 10^4 counts around that region, it will be impossible to resolve this peak. The solution around this problem will be to use more that 3 grams of vanadium sample but this could not be obtained at the time of this report.

Detection system and shielding issues

The absolute efficiency of our detection system was low compared to other facilities. Our detection efficiency at about 1.4 MeV is a factor of 100 lower than the facility at the University of Texas at Austin (Revay et al. 2007). Geometric efficiency of about 0.009 could have been improved upon but without an excellent reduction in background, then a higher signal-to-noise ratio would not be achieved. Acquiring a detector with much better efficiency can offer some improvement. Germanium peaks in the spectrum can be detrimental due to the loss of resolution of the detection system. Another issue of concern is the damage to the crystal, very common to p-type detectors. Inadequate shielding can be attributable to this. The end cap of the HPGe was not properly shielded during these investigations as evident in the germanium and aluminum peaks. The choice material of enriched ^{6}Li required to absorb scattered neutrons could not be obtained. Attempts to cover the HPGe end cap with a layer of natural Li_2CO_3 powder did reduce the peak area counts on the 595 keV principal peaks, but this also attenuated the

gamma-ray energies greatly. Fig 4-10 shows poly bags filled with natural lithium carbonate powder obtained from the NSC and covering around the cryostat of the HPGe. When Li_2CO_3 powder was used to cover all sides of the cryostat with about 3 cm thickness covering the end cap of the detector the 244 keV peak from ^{152}Eu could not be resolved in the spectrum and more counts on the prompt peak from hydrogen were observed during irradiation. With the lithium carbonate lid present at 21.5 inches sample-to-detector distance, the 595 keV Ge peak counts for 300 seconds irradiation was reduced from 65 cps to 14 cps, with the prompt H peak counts increased from 8.4 to 14.4 cps. Reducing the thickness of Li_2CO_3 will reduce the attenuation of gamma rays with a consequent reduction of the number of atoms of ^6Li. Natural Li_2CO_3 powder contains about 7 % of ^6Li atoms which is why this application requires a smaller thickness enriched in ^6Li isotope.

Fig 4-10. Shielding improvements with natural lithium carbonate powder.

CHAPTER V

CONCLUSIONS

A prompt-gamma, neutron-activation analysis facility was developed at BP #1 on the Lower Research Level of the NSC reactor. Neutron beams from the reactor core were filtered using a sapphire crystal placed in the graphite plug inside the beam port towards the reactor core. This improved the cadmium ratio from about 6 to 122, but with a substantial reduction in thermal neutron fluence rate from 8.758 x 10^6 n cm^{-2} s^{-1} to 9.3 x10^5 n cm^{-2} s^{-1} at the sample position. The gamma and neutron exposure rates around the lower research level were reduced by a factor of ten and twenty respectively and were within facility administrative limits. The divergence of the neutron beam was minimal with the introduction of a new collimator.

The efficiency of the detector was determined using a ^{152}Eu calibration point source obtained from NIST. A theoretical model was developed and used to predict the net peak area counts expected in the most intense prompt gamma-ray peaks of chlorine and cadmium. The predictive model used the measured neutron fluence rate, calculated detector efficiencies, the mass of the sample, and the partial capture cross section data for each element. Cadmium and chlorine were chosen for this investigation because majority of their intense prompt gamma-ray energies fall within the range of our calibration source energies and they have an appreciable thermal neutron cross section.

The performance capability of the facility was examined by comparing the predicted and experimentally measured net peak area counts of the different prompt gamma-ray energies. Within limits of our experimental errors, the discrepancies between

the predicted and experimentally measured net peak area counts on the most intense prompt peaks of chlorine were minimal. Because of the effects of self shielding which was expected from cadmium, the discrepancies observed between cadmium measurements and predictions were larger than for chlorine. By applying corrections for self-shielding to predicted values, the observed discrepancies were reduced.

Experimental results validated the predictive calculations using our model. Once corrections for self absorption and self-shielding were applied, discrepancies between measured and predicted net peak area counts agreed to within a factor of two or less. Another application of our predictive model was its usefulness in determining the mass of sample and irradiation duration expected to obtain desired counts at the peak; and this is done even before the experiment is initiated. This is very useful to a multi-user facility like the NSC to help with efficient allocation of beam time. However, this model cannot achieve this feat for samples with unknown elemental concentrations.

We have established the practical significance of our PGNAA facility through the results of our analysis of the peak area counts per prompt gamma-ray energy. However, the present facility cannot be used for precise analysis of boron and hydrogen, especially for samples with trace quantities, due to the high background counts already identified in the spectrum. The acquisition electronics also cannot allow for longer irradiation duration. The acquisition duration during these investigations were limited to about an hour; improved acquisition electronics are required. A high gamma background counts from the reactor gamma radiation needs shielding improvements especially for lower energies. The facility does not have the capability to efficiently analyze samples with prompt gamma-ray energies below 500 keV due to the high Compton continuum from

the reactor gamma radiation. Germanium and lead peaks are present in the spectrum. This is a strong evidence of scattered neutrons reaching the detector and shielding materials. This could lead to loss of resolution and crystal damage if not addressed; improvements in neutron shielding are required along with shielding to reduce reactor gamma radiation. The neutron flux from the NSC reactor is low; improvements are needed to reduce the irradiation times and improve analytical sensitivities.

Quantitative analysis of samples with prompt gamma- energies above 2 MeV will not be possible without energy and efficiency calibration in that range. The detection efficiency at 1.4 MeV was rather small due to a low-efficiency detector and a poor geometric efficiency introduced by a sample-to-detector distance of 55 cm. As we observed, this efficiency is lower than peer facilities by about a factor of 100 and it needs improvement. Whereas excellent shielding of reactor gamma rays can reduce the background and hence give room for a reduction in the sample-to-detector distance, acquisition of a highly efficient detector with excellent resolution will improve the system.

This study has provided a theoretical approach to validating the performance capability of the PGNAA facility at the Nuclear Science Center. Improvements in shielding materials around the sample chamber, beam stop, and detector as well as acquisition of an efficient detector with good resolution should be considered. An MCNP model of the facility can give insight on shielding improvements. It was observed that scattered neutrons still reached the detector. This can be corrected using ^{6}Li-based shielding materials. Improved detection electronics and a modern personal computer that can allow for efficient acquisition of spectrum should be acquired to replace the present

computer. A Compton suppression detection system can be incorporated in the improvements, but in-depth studies into methods of reducing the gamma background of the reactor should be a priority.

Overall, our investigation has shown that there are unexploited possibilities of the PGNAA facility in complementing the existing NAA capabilities of the NSC.

REFERENCES

Adib M, Kilany M, Habib N, Fathallah M. Neutron transmission of single-crystal sapphire filters. Czech J Phys 55: 563-578; 2005.

Alfassi ZB and Chung C, eds. Prompt gamma neutron activation analysis. Boca Raton, FL: CRC Press; 1995.

Anderson DL, Mackey EA. Improvements in food analysis by thermal neutron capture prompt gamma-ray spectrometry. J of Radioanal Nucl Ch 263: 683-689; 2005.

Anderson DL, Failey MP, Zoller WH, Walters WB, Gordon GE, Lindstrom RM. Facility for non-destructive analysis for major and trace elements using neutron-capture gamma-ray spectrometry. J of Radioanal Chem 63: 97-119; 1981a.

Anderson DL, Zoller WH, Gordon, GE, Walters WB. Neutron-capture prompt gamma-ray spectrometry as a quantitative analytical method. Proceedings of the 4^{th} (n, γ) International Symposium. Grenoble: Institute of Physics Conference Series 62: 7-11; 1981b.

Belgya T, Revay Zs. Principles of the PGAA method In: Molnar GL, ed. Handbook of prompt gamma activation analysis with neutron beams. Dordrecht, The Netherlands: Kluwer Academic Publishers; 2004: 1-30.

Belgya T, Revay Zs. Gamma-Ray Spectrometry In: Molnar GL, ed. Handbook of prompt gamma activation analysis with neutron beams. Dordrecht, The Netherlands: Kluwer Academic Publishers; 71-111. 2004.

Byun SH, Sun GM, Choi HD. Development of a prompt gamma activation analysis facility using diffracted polychromatic neutron beam. Nucl Instrum Methods Phys Res A 487: 521-529; 2002.

Glascock MD. Practical applications of neutron capture reactions and prompt gamma rays. Proceedings of the 4^{th} (n, γ) International Symposium. Grenoble: Institute of Physics Conference Series 62: 641; 1981.

Glascock MD. Overview of neutron activation analysis. Archaeometry Laboratory, University of Missouri Research reactor. Available at http://archaeometry.missouri.edu/ naa_ overview.html. Accessed 12 April 2008.

Hanna AG, Brugger RM, Glascock MD. The prompt gamma neutron activation analysis facility at MURR. Nucl Instrum Methods 188:619-627; 1981.

Harling OK, Chabeuf JM, Lambert F, Yasuda G. A prompt gamma neutron activation analysis facility using a diffracted beam. Nucl Instrum Methods Phys Res B 83:557-562; 1993.

Isenhour TL, Morrison GH. Modulation technique for neutron capture gamma ray measurements in activation analysis. Anal Chem 38:162-167; 1966a.

Isenhour TL, Morrison GH. Determination of boron by thermal neutron activation analysis using a modulated technique. Anal Chem 38:167-169; 1966b.

Khalil, SN. Design, Installation and implementation of a neutron depth profiling facility at the Texas A&M Nuclear Science Center. M.S. thesis, Department of Nuclear Engineering; Texas A&M University, College Station; 1989.

Knoll GF. Radiation detection and measurement, 3rd ed. New York: John Wiley & Sons; 1999.

Krohn JL. Development and application of a prompt gamma activation analysis in the measurement of neutron capture cross-sections of geologic materials. Ph.D. dissertation, Department of Nuclear Engineering; Texas A&M University, College Station; 1992.

Lindstrom RM, Anderson DL. Analytical neutron-capture gamma-ray spectroscopy: Status and prospects. In: Raman S, ed. Capture gamma spectroscopy and related topics-1984, New York: American Institute of Physics; 1985: 180.

Lindstrom RM, Revay Zs. Beams and facilities In: Molnar GL, ed. Handbook of prompt gamma activation analysis with neutron beams. Dordrecht, The Netherlands: Kluwer Academic Publishers; 2004: 31-58.

Lombard SM, Isenhour TL, Heintz PH, Woodruff GL, Wilson WE. Neutron capture gamma-ray activation analysis: design of apparatus for trace analysis. Int J Appl Radiat Isot 19: 15-22; 1968.

Mackey EA, Anderson DL, Liposky PJ, Lindstrom RM, Chen-Mayer H, Lamaze GP. New thermal neutron prompt gamma-ray activation analysis facility at the National Institute of Standards and technology center for neutron research. Nucl Instrum Methods Phys Res B 226: 426–440; 2004.

Molnar GL, Revay Zs, Belgya T. Wide energy range efficiency calibration method for Ge detectors. Nucl Instrum Methods Phys Res A 489: 140–159; 2002.

Molnar GL, Revay Zs, Paul RL, Lindstrom RM. Prompt-gamma activation analysis using the k_0 approach. J Radioanal Nucl Ch 234: 21-26; 1998.

Molnar GL. Nuclear data for activation analysis. J of Radioanal Nucl Ch 244: 27-33; 2000.

PGAA Prompt gamma data [database online] IAEA, Vienna; 2003. Available at http:/ www-nds.iaea.org/pgaa/databases.htm. Accessed 15 May 2007.

Revay Zs, Firestone RB, Belgya,T, Molnar GL. Prompt gamma-ray spectrum catalog In: Molnar GL, ed. Handbook of prompt gamma activation analysis with neutron beams. Dordrecht, The Netherlands: Kluwer Academic Publishers; 2004: 173-364.

Revay Zs, Harrison RK, Alvarez E, Biegalski SR, Landsberger S. Construction and characterization of the redesigned PGAA facility at the University of Texas at Austin. Nucl Instrum Methods Phys Res A 577: 611–618; 2007.

Szentmiklosi L, Gmeling K, Revay Zs. Fitting the boron peak and resolving interferences in the 450-490 keV region of PGAA spectra. J Radioanal Nucl Ch 271: 447-453; 2007.

Yonezawa C. Quantitative analysis In: Molnar GL, ed. Handbook of prompt gamma activation analysis with neutron beams. Dordrecht, The Netherlands: Kluwer Academic Publishers; 2004: 113-135.

APPENDIX A

BACKGROUND SPECTRUM PEAK SEARCHES

Appendix A-1. Facility Background Peak Search Results-3099 secs. (No neutron beam)

```
**************************************************************************
*****           P E A K    A N A L Y S I S    R E P O R T           *****
**************************************************************************

     Detector Name:  DET01
     Sample Title:   BG_24APR08
     Peak Analysis Performed on:  5/12/2008   1:12:38 PM
               Peak Analysis From Channel:      1
               Peak Analysis To Channel:    16384
```

Peak No.	ROI start	ROI end	Peak centroid	Energy (keV)	FWHM (keV)	Net Peak Area	Net Area Uncert.	Continuum Counts
1	88-	101	95.23	182.07	5.30	1.04E+005	758.39	1.56E+005
2	381-	392	384.53	433.95	2.95	5.96E+003	582.62	1.33E+005
3	465-	480	472.87	510.86	4.05	7.60E+005	1014.27	8.98E+004
4	584-	599	591.38	614.04	3.56	6.64E+003	329.07	3.38E+004
5	707-	724	716.05	722.58	3.63	7.29E+003	282.66	2.23E+004
6	775-	787	779.41	777.74	4.27	4.82E+002	186.65	1.30E+004
7	988-	1002	993.31	963.97	4.20	5.45E+002	161.84	8.89E+003
8	1127-	1140	1134.07	1086.52	1.92	4.31E+002	134.37	6.39E+003
9	1158-	1172	1163.09	1111.78	4.11	4.84E+002	136.90	6.33E+003
10	1230-	1243	1234.20	1173.69	3.06	3.50E+002	119.21	5.02E+003
11	1364-	1382	1372.70	1294.27	4.23	3.49E+003	147.49	5.40E+003
12	1411-	1426	1417.81	1333.55	2.99	3.18E+002	111.33	4.02E+003
13	1498-	1511	1504.15	1408.72	4.72	6.73E+002	96.38	3.12E+003

```
M = First peak in a multiplet region
m = Other peak in a multiplet region
F = Fitted singlet

Errors quoted at  1.000 sigma
```

Appendix A-2. PGNAA Background Peak Search Results -3602 secs.

```
*************************************************************************
*****          P E A K   A N A L Y S I S   R E P O R T           *****
*************************************************************************

     Detector Name:  DET01
     Sample Title:   CFA_25APR08
     Peak Analysis Performed on:  4/25/2008   4:45:12 PM
               Peak Analysis From Channel:      1
               Peak Analysis To Channel:    16384
```

	Peak No.	ROI start	ROI end	Peak centroid	Energy (keV)	FWHM (keV)	Net Peak Area	Net Area Uncert.	Continuum Counts
M	1	69-	101	75.97	166.14	6.51	1.15E+004	255.41	7.03E+004
m	2	69-	101	84.22	173.31	6.52	6.60E+004	510.54	4.53E+005
m	3	69-	101	94.45	182.19	6.51	7.97E+005	1611.45	1.40E+006
	4	106-	119	112.81	198.14	5.53	1.55E+005	2836.19	2.86E+006
	5	169-	183	176.16	253.17	4.43	4.17E+004	2803.56	2.71E+006
	6	223-	234	227.13	297.44	4.81	2.57E+004	2276.64	2.05E+006
	7	255-	267	260.58	326.50	3.99	4.18E+004	2306.81	2.00E+006
	8	426-	441	434.02	477.14	10.84	1.84E+006	2701.35	1.82E+006
M	9	451-	480	464.97	504.02	3.35	2.26E+005	921.73	8.57E+005
m	10	451-	480	472.52	510.58	5.06	3.74E+006	2219.15	1.13E+006
M	11	518-	555	540.50	569.63	3.27	-3.95E+002	1463.06	4.33E+005
m	12	518-	555	546.81	575.11	3.28	-3.39E+002	1257.16	3.88E+005
M	13	562-	592	570.43	595.62	4.98	1.11E+005	733.72	5.32E+005
m	14	562-	592	583.81	607.25	5.00	2.69E+004	563.99	5.03E+005
M	15	674-	724	684.34	694.57	8.87	4.18E+004	657.33	4.93E+005
m	16	674-	724	698.14	706.56	8.87	3.72E+004	633.46	5.82E+005
m	17	674-	724	715.20	721.37	8.88	8.24E+003	561.47	4.49E+005
	18	741-	752	744.27	746.62	3.17	2.23E+003	684.64	1.86E+005
	19	799-	816	808.28	802.22	5.00	1.24E+004	884.32	2.37E+005
M	20	833-	863	842.34	831.80	8.18	9.08E+003	492.73	2.95E+005
m	21	833-	863	854.29	842.18	8.19	8.24E+003	484.51	2.92E+005
	22	874-	891	883.00	867.12	4.44	2.82E+004	831.29	2.04E+005
	23	908-	925	916.71	896.40	4.77	5.34E+003	782.04	1.86E+005
M	24	984-	1022	990.20	960.24	4.30	3.50E+003	329.90	1.25E+005
m	25	984-	1022	1006.65	974.52	4.32	1.37E+003	284.76	1.39E+005
m	26	984-	1022	1013.27	980.27	4.32	1.43E+003	287.49	1.37E+005
	27	1102-	1117	1108.52	1063.00	2.84	1.97E+003	593.10	1.16E+005
	28	1136-	1155	1146.15	1095.70	7.12	1.39E+004	716.26	1.42E+005
	29	1191-	1202	1195.15	1138.25	4.66	3.84E+003	444.80	7.72E+004
	30	1259-	1278	1269.04	1202.43	7.78	1.51E+004	656.73	1.19E+005
	31	1362-	1382	1372.51	1292.30	6.04	2.79E+004	654.98	1.11E+005
	32	1464-	1480	1470.21	1377.17	5.57	3.75E+003	502.26	7.93E+004
	33	1558-	1574	1568.07	1462.17	5.04	4.45E+003	491.72	7.58E+004
	34	1644-	1653	1648.31	1531.86	1.32	5.72E+002	303.26	4.04E+004
	35	1718-	1731	1722.56	1596.36	1.62	2.04E+002	388.68	5.47E+004
M	36	1827-	1880	1837.33	1696.04	8.46	3.27E+003	254.26	8.73E+004
m	37	1827-	1880	1853.37	1709.98	8.47	5.76E+003	270.97	1.04E+005
m	38	1827-	1880	1869.66	1724.13	8.48	3.43E+003	255.28	8.94E+004
	39	1920-	1940	1930.82	1777.25	6.25	5.94E+003	514.65	7.13E+004
	40	2061-	2070	2065.56	1894.28	1.19	2.73E+001	269.14	3.20E+004
	41	2431-	2453	2442.49	2221.68	7.52	5.15E+004	530.68	5.94E+004
	42	2881-	2903	2892.42	2612.49	7.36	2.43E+003	407.85	4.22E+004
	43	3330-	3340	3335.89	2997.68	1.80	-1.08E+002	197.66	1.64E+004
	44	4676-	4689	4682.73	4167.53	4.07	4.68E+002	193.87	1.35E+004

Appendix A-2 Continued.

	Peak No.	ROI start	ROI end	Peak centroid	Energy (keV)	FWHM (keV)	Net Peak Area	Net Area Uncert.	Continuum Counts
	45	6183-	6199	6190.68	5477.32	2.28	2.56E+002	197.48	1.24E+004
M	46	6387-	6463	6392.87	5652.94	5.22	2.18E+002	88.64	1.02E+004
m	47	6387-	6463	6429.09	5684.41	5.23	4.62E+002	92.79	1.33E+004
m	48	6387-	6463	6454.43	5706.41	5.24	4.46E+002	99.33	1.36E+004
	49	6598-	6611	6604.15	5836.46	2.57	4.14E+001	159.98	9.26E+003
M	50	7157-	7202	7173.90	6331.34	10.41	8.76E+003	185.50	2.31E+004
m	51	7157-	7202	7186.88	6342.61	10.41	8.19E+003	181.93	2.33E+004
	52	7222-	7235	7228.84	6379.05	1.62	3.22E+002	166.98	9.99E+003
	53	7477-	7502	7488.96	6604.99	5.56	1.09E+003	279.24	1.81E+004
	54	7754-	7787	7770.75	6849.76	17.45	1.47E+004	354.42	2.11E+004
M	55	8059-	8103	8074.63	7113.70	13.26	1.79E+003	153.70	1.61E+004
m	56	8059-	8103	8090.74	7127.70	13.27	9.65E+002	133.50	1.47E+004
	57	8259-	8278	8266.52	7280.37	1.07	3.32E+001	127.18	4.61E+003
	58	8345-	8378	8362.31	7363.58	10.72	9.51E+003	248.22	1.00E+004
	59	8399-	8427	8410.37	7405.32	8.02	8.27E+002	166.61	5.82E+003
M	60	8646-	8692	8661.09	7623.10	13.79	1.16E+003	88.20	5.29E+003
m	61	8646-	8692	8678.28	7638.03	13.79	7.33E+002	79.54	5.15E+003
	62	9495-	9511	9502.21	8353.68	1.51	5.53E-001	55.28	9.69E+002

M = First peak in a multiplet region
m = Other peak in a multiplet region
F = Fitted singlet

Errors quoted at 1.000 sigma

Appendix A-3. Peak identification for beam background spectrum

Energy(keV)	Net Peak Area	Counts per seconds	Identification
166.14	1.15E+04	3.19	?
173.31	6.60E+04	18.32	^{71mGe} IT @175.08 keV *
182.19	7.97E+05	221.27	?
198.14	1.55E+05	43.03	^{19F} @ 197.29 keV *
253.17	4.17E+04	11.58	^{75}Ge @ 253.32 keV (n,γ)
297.44	2.57E+04	7.13	^{73}Ge @ 297.36 keV (n,γ)
326.5	4.18E+04	11.60	^{73}Ge @ 325.88 keV (n,γ)
477.14	1.84E+06	510.83	B(n,α)^{7}Li
504.02	2.26E+05	62.74	?
510.58	3.74E+06	1038.31	Annihilation peak
569.63	-3.95E+02	0.00	Error
575.11	-3.39E+02	0.00	Error
595.62	1.11E+05	30.82	^{74}Ge @ 595.86 keV (n,γ)
607.25	2.69E+04	7.47	^{74}Ge @ 608.30 keV (n, n′γ)
694.57	4.18E+04	11.60	^{72}Ge,Fe @ 693.05 keV (n, n′γ)
706.56	3.72E+04	10.33	^{71}Ge @ 708.40 keV (n,γ)
721.37	8.24E+03	2.29	?
746.62	2.23E+03	0.62	?
802.22	1.24E+04	3.44	^{206}Pb @ 803.2 keV (n, n′γ)
831.8	9.08E+03	2.52	^{28}Al @ 831.8 keV (n, n′γ)
842.18	8.24E+03	2.29	^{27}Al @ 843.5 keV (n, n′γ)
867.12	2.82E+04	7.83	^{73}Ge major peak
896.4	5.34E+03	1.48	^{207}Pb @ 896.56 keV (n, n′γ)
960.24	3.50E+03	0.97	^{73}Ge @ 961.055 keV major peak
974.52	1.37E+03	0.38	?
980.27	1.43E+03	0.40	?
1063	1.97E+03	0.55	?
1095.7	1.39E+04	3.86	^{70}Ge
1138.25	3.84E+03	1.07	?, ^{70}Ge @ 1139.27 keV
1202.43	1.51E+04	4.19	H single escape peak 1201.38 keV
1292.3	2.79E+04	7.75	^{41}Ar
1377.17	3.75E+03	1.04	?
1462.17	4.45E+03	1.24	?
1531.86	5.72E+02	0.16	?
1596.36	2.04E+02	0.06	?
1696.04	3.27E+03	0.91	?
1709.98	5.76E+03	1.60	?
1724.13	3.43E+03	0.95	?
1777.25	5.94E+03	1.65	^{28}Al @ 1778.92 keV activation
1894.28	2.73E+01	0.01	?

Appendix A-3. Continued

Energy(keV)	Net Peak Area	Counts per seconds	Identification
2221.68	5.15E+04	14.30	H (n,γ)
2612.49	2.43E+03	0.67	^{208}Pb @ 2614.58 keV (n, n′γ)
2997.68	-1.08E+02	0.00	Error
4167.53	4.68E+02	0.13	?
5477.32	2.56E+02	0.07	?
5652.94	2.18E+02	0.06	?
5684.41	4.62E+02	0.13	?
5706.41	4.46E+02	0.12	?
5836.46	4.14E+01	0.01	?
6331.34	8.76E+03	2.43	?
6342.61	8.19E+03	2.27	?
6379.05	3.22E+02	0.09	?
6604.99	1.09E+03	0.30	?
6849.76	1.47E+04	4.08	?
7113.7	1.79E+03	0.50	?
7127.7	9.65E+02	0.27	?
7280.37	3.32E+01	0.01	?
7363.58	9.51E+03	2.64	^{207}Pb @7367.78 keV (n, n′γ) *
7405.32	8.27E+02	0.23	?
7623.1	1.16E+03	0.32	?
7638.03	7.33E+02	0.20	?
8353.68	5.53E-01	0.00	?

***** Denotes that the peak is questionable

? Denotes that the peak could not be identified, but it appears in the spectrum

APPENDIX B

NIST CERTIFICATE FOR SRM 4370C - ^{152}EU

S. Department of Commerce
Malcolm Baldrige
Secretary

National Bureau of Standards
Ernest Ambler, Director

National Bureau of Standards

Certificate

Standard Reference Material 4370C

Radioactivity Solution Standard

Radionuclide	Europium-152
Source identification	4370C
Source description	Liquid in 5-mL flame-sealed glass ampoule (1)*
Source mass	5.0338 ± 0.0019 grams (2)
Solution composition	277 µg Eu per gram of 1 M HCl
Radioactivity concentration	9.390×10^{4} Bq g^{-1}
Reference time	1200 EST February 2, 1987
Overall uncertainty	1.1 percent (3)
Photon-emitting impurities (activity ratio at reference time)	$^{154}Eu/^{152}Eu$: $(2.9 \pm 0.3) \times 10^{-3}$ (4)
Half life	13.55 ± 0.06 years (5)
Measuring instrument	4πγ pressurized ionization-chamber "A" previously standardized by 4πγ counting with the NBS 8"x8" NaI(Tl) crystals

This Standard Reference Material was prepared in the Center for Radiation Research, Ionizing Radiation Division, Radioactivity Group, Dale D. Hoppes, Group Leader.

Gaithersburg, MD 20899
March, 1987

Stanley D. Rasberry, Chief
Office of Standard Reference Materials

*Notes on back

National Bureau of Standards Certificate Data
Standard Reference Material 4370C
NSC Property Number 10146

Isotope	Eu-152			
Halflife	13.55 years	+/-	0.06 years	
Radioassay Date	2-Feb-87 12:00			
Source Mass	5.0338 grams	+/-	0.0019 grams	
Activity Concentraion	9.39E+04 Bq/gram	+/-	1032.9 Bq (1.1%)	
Source Activity	472673.82 Bq	+/-	5202.5 Bq	
	12.775 uCi	+/-	0.141 uCi	

Energy (KeV)	%Abn	GPS	Uncertainty (+/-)	% Err
121.78	28.40	134239.36	1477.50	1.101
244.69	7.49	35403.27	389.67	1.101
344.27	26.50	125258.56	1378.66	1.101
411.11	2.21	10446.09	114.97	1.101
443.98	3.11	14700.16	161.80	1.101
778.89	12.74	60218.64	662.79	1.101
867.32	4.16	19663.23	216.42	1.101
964.01	14.40	68065.03	749.16	1.101
1085.78	10.00	47267.38	520.25	1.101
1112.02	13.30	62865.62	691.93	1.101
1407.95	20.70	97843.48	1076.91	1.101

APPENDIX C

PEAK SEARCH FOR CHLORINE AND CADMIUM

Appendix C-1. Peak Search for Chlorine irradiation – 2001.2 seconds

```
**************************************************************************
*****          P E A K   A N A L Y S I S   R E P O R T           *****
**************************************************************************

     Detector Name:  DET01
     Sample Title:   NACL_24APR08
     Peak Analysis Performed on:  5/12/2008   1:17:20 PM
               Peak Analysis From Channel:      1
               Peak Analysis To Channel:    16384
```

	Peak No.	ROI start	ROI end	Peak centroid	Energy (keV)	FWHM (keV)	Net Peak Area	Net Area Uncert.	Continuum Counts
M	1	69-	101	75.74	165.10	6.29	1.99E+003	270.09	2.57E+004
m	2	69-	101	81.80	170.38	6.28	1.32E+004	326.80	1.02E+005
m	3	69-	101	94.18	181.16	6.29	3.80E+005	871.45	6.40E+005
	4	106-	119	113.01	197.55	5.69	2.20E+005	1905.76	1.24E+006
	5	169-	183	176.45	252.79	4.00	5.16E+004	1835.74	1.15E+006
M	6	198-	234	204.36	277.09	4.93	8.68E+003	811.42	1.11E+006
m	7	198-	234	212.16	283.88	4.94	8.16E+003	797.00	1.62E+006
m	8	198-	234	227.00	296.80	4.97	3.54E+004	852.07	1.60E+006
	9	253-	267	260.12	325.63	4.46	6.84E+004	1704.24	9.84E+005
	10	283-	298	290.89	352.42	6.11	4.16E+003	1620.18	8.72E+005
	11	334-	343	336.19	391.86	3.05	3.39E+003	1033.43	4.71E+005
	12	380-	393	385.92	435.16	2.26	4.97E+003	1268.74	5.82E+005
	13	426-	441	434.19	477.18	10.74	6.77E+005	1772.88	8.21E+005
M	14	452-	480	460.69	500.26	3.66	7.28E+004	586.25	5.54E+005
m	15	452-	480	472.92	510.90	5.37	1.42E+006	1229.73	8.63E+005
	16	538-	552	546.54	575.00	4.22	7.29E+003	901.22	2.79E+005
M	17	562-	593	570.55	595.90	4.59	1.46E+005	532.98	3.06E+005
m	18	562-	593	584.79	608.30	4.60	2.23E+004	392.12	3.39E+005
	19	608-	620	612.68	632.58	4.31	3.25E+003	718.04	1.94E+005
M	20	663-	724	685.08	695.61	6.67	1.38E+004	379.42	4.36E+005
m	21	663-	724	698.98	707.72	6.69	3.94E+004	429.18	4.35E+005
m	22	663-	724	716.52	722.99	6.71	4.00E+003	349.70	3.84E+005
	23	740-	752	744.15	747.04	3.50	1.29E+003	624.51	1.47E+005
	24	782-	799	790.71	787.58	5.42	7.62E+004	847.07	1.97E+005
	25	805-	822	814.40	808.21	3.82	6.94E+003	778.30	1.84E+005
	26	832-	849	840.83	831.22	5.20	9.49E+003	774.99	1.81E+005
M	27	874-	911	883.15	868.06	4.85	4.18E+004	352.92	1.78E+005
m	28	874-	911	903.14	885.46	4.86	1.74E+003	281.20	2.10E+005
M	29	948-	972	954.45	930.13	5.94	2.28E+003	315.67	1.51E+005
m	30	948-	972	963.70	938.19	5.95	3.81E+003	321.70	2.21E+005
	31	982-	999	990.67	961.67	3.79	5.63E+003	706.71	1.52E+005
	32	1030-	1042	1033.86	999.27	3.63	1.87E+003	520.08	1.02E+005
	33	1101-	1116	1110.37	1065.89	3.43	1.44E+003	587.23	1.14E+005
	34	1138-	1156	1147.51	1098.22	8.98	1.77E+004	696.05	1.38E+005
M	35	1176-	1203	1185.90	1131.64	4.91	5.75E+003	244.81	1.28E+005

Appendix C-1 Continued

	Peak No.	ROI start	ROI end	Peak centroid	Energy (keV)	FWHM (keV)	Net Peak Area	Net Area Uncert.	Continuum Counts
m	36	1176-	1203	1195.12	1139.67	4.92	8.09E+003	257.61	1.55E+005
	37	1215-	1234	1224.57	1165.31	5.41	6.13E+004	729.48	1.34E+005
	38	1260-	1279	1269.90	1204.77	6.09	1.84E+004	679.67	1.26E+005
	39	1319-	1331	1323.93	1251.81	3.52	1.17E+003	457.89	7.91E+004
	40	1366-	1385	1375.80	1296.97	10.14	2.04E+004	652.78	1.16E+005
	41	1406-	1419	1411.83	1328.35	4.96	1.02E+003	467.95	7.90E+004
	42	1461-	1480	1470.86	1379.74	5.95	7.06E+003	618.84	1.07E+005
M	43	1558-	1586	1568.32	1464.59	5.67	1.07E+004	240.94	1.09E+005
m	44	1558-	1586	1578.26	1473.24	5.68	2.88E+003	221.95	1.39E+005
	45	1715-	1733	1726.21	1602.06	6.12	7.50E+003	562.72	9.14E+004
	46	1829-	1847	1837.25	1698.73	4.99	2.44E+003	555.42	9.05E+004
M	47	1902-	1941	1906.80	1759.28	5.93	7.36E+002	200.78	6.94E+004
m	48	1902-	1941	1930.98	1780.33	5.94	7.30E+003	235.28	1.34E+005
M	49	2118-	2151	2129.76	1953.40	6.38	2.55E+004	263.00	9.76E+004
m	50	2118-	2151	2139.52	1961.89	6.38	1.68E+004	247.26	1.38E+005
	51	2219-	2235	2224.60	2035.97	4.24	1.94E+003	440.96	6.15E+004
	52	2431-	2454	2442.85	2225.98	7.29	2.58E+004	589.24	8.03E+004
	53	3168-	3192	3180.26	2867.99	7.19	5.53E+003	506.27	6.07E+004
	54	3394-	3419	3407.24	3065.60	8.72	2.57E+003	499.09	5.80E+004
	55	4425-	4446	4439.42	3964.25	2.88	1.49E+003	367.92	3.56E+004
	56	5633-	5662	5647.68	5016.19	6.77	1.47E+003	430.58	3.87E+004
	57	5721-	5751	5736.46	5093.49	16.05	6.62E+003	458.93	4.18E+004
	58	5857-	5884	5872.45	5211.88	5.17	1.90E+003	403.80	3.58E+004
	59	6221-	6243	6235.76	5528.19	3.09	8.69E+002	328.99	2.77E+004
	60	6311-	6341	6326.35	5607.07	13.73	1.03E+004	446.46	3.87E+004
	61	6423-	6437	6429.74	5697.08	1.24	-1.78E+002	227.87	1.81E+004
	62	6899-	6930	6915.22	6119.75	12.06	9.86E+003	406.70	3.11E+004
M	63	7090-	7119	7096.60	6277.66	2.45	2.15E+002	63.71	9.00E+003
m	64	7090-	7119	7110.70	6289.94	2.46	2.24E+002	63.51	8.86E+003
M	65	7161-	7250	7175.71	6346.54	6.63	1.74E+003	103.29	2.21E+004
m	66	7161-	7250	7187.81	6357.07	6.64	1.79E+003	110.42	3.20E+004
m	67	7161-	7250	7229.34	6393.23	6.65	1.97E+003	114.44	4.18E+004
m	68	7161-	7250	7241.42	6403.75	6.65	2.67E+003	131.64	4.04E+004
	69	7320-	7339	7326.24	6477.59	4.55	3.53E+002	230.92	1.51E+004
	70	7489-	7521	7505.49	6633.66	5.78	3.10E+003	358.53	2.45E+004
M	71	7742-	7788	7761.63	6856.66	7.53	1.59E+003	124.56	1.91E+004
m	72	7742-	7788	7774.81	6868.13	7.54	3.60E+003	164.57	2.65E+004
	73	7807-	7840	7824.00	6910.96	18.12	4.86E+003	337.53	2.08E+004
	74	8013-	8028	8021.05	7082.52	1.06	2.40E+001	151.06	7.57E+003
	75	8253-	8274	8260.98	7291.40	1.56	6.04E+002	181.59	8.59E+003
	76	8346-	8377	8362.97	7380.20	9.15	2.43E+003	236.52	1.07E+004
	77	8398-	8431	8415.02	7425.52	12.01	3.50E+003	246.94	1.09E+004
	78	8552-	8569	8562.63	7554.03	1.88	1.57E+002	122.13	4.52E+003
	79	8830-	8864	8847.41	7801.97	10.16	1.57E+003	191.08	6.50E+003
	80	9552-	9568	9560.40	8422.72	4.05	1.33E+002	67.88	1.43E+003
	81	10438-	10457	10445.55	9193.35	1.91	8.69E+000	45.55	5.88E+002
	82	11490-	11505	11497.30	10109.03	0.92	2.23E+001	16.93	8.67E+001

M = First peak in a multiplet region
m = Other peak in a multiplet region
F = Fitted singlet

Errors quoted at 1.000 sigma

Appendix C-2. Peak Search for Cadmium irradiation – 2001.6 seconds

```
**************************************************************************
*****          P E A K   A N A L Y S I S   R E P O R T           *****
**************************************************************************

     Detector Name:  DET01
     Sample Title:   CD_2_24APR08
     Peak Analysis Performed on:  5/12/2008   1:15:16 PM
               Peak Analysis From Channel:      1
               Peak Analysis To Channel:    16384
```

	Peak No.	ROI start	ROI end	Peak centroid	Energy (keV)	FWHM (keV)	Net Peak Area	Net Area Uncert.	Continuum Counts
M	1	69-	101	76.16	165.47	6.21	2.54E+003	244.78	2.60E+004
m	2	69-	101	82.45	170.95	6.22	1.49E+004	335.46	1.31E+005
m	3	69-	101	94.33	181.30	6.22	3.77E+005	876.94	6.49E+005
	4	106-	119	112.99	197.54	5.53	2.18E+005	1926.47	1.27E+006
	5	169-	183	176.40	252.74	4.07	5.44E+004	1857.15	1.18E+006
	6	201-	211	204.79	277.46	1.88	2.55E+003	1416.97	8.40E+005
M	7	220-	245	227.36	297.11	5.15	3.79E+004	822.73	1.25E+006
m	8	220-	245	237.85	306.24	5.17	1.58E+004	793.45	1.67E+006
	9	253-	267	260.18	325.69	4.51	6.74E+004	1731.70	1.02E+006
	10	289-	298	291.08	352.59	2.58	4.82E+003	1133.34	5.66E+005
	11	328-	343	336.17	391.85	3.97	6.07E+003	1552.79	8.00E+005
	12	362-	371	364.45	416.47	5.95	8.78E+003	1019.45	4.56E+005
	13	426-	442	434.33	477.30	10.97	7.10E+005	1815.39	8.27E+005
M	14	452-	480	460.80	500.35	3.63	8.28E+004	590.74	5.49E+005
m	15	452-	480	472.83	510.83	5.34	1.44E+006	1218.32	7.92E+005
M	16	519-	555	527.38	558.32	4.34	2.34E+005	632.93	3.59E+005
m	17	519-	555	547.26	575.63	4.36	1.70E+004	418.37	3.90E+005
M	18	562-	593	570.54	595.89	4.61	1.47E+005	542.87	3.25E+005
m	19	562-	593	584.70	608.22	4.62	2.22E+004	403.89	3.62E+005
	20	605-	617	612.76	632.65	2.94	1.34E+003	752.62	2.15E+005
	21	625-	642	634.03	651.17	4.54	4.71E+004	978.99	2.80E+005
M	22	675-	726	684.54	695.14	6.50	1.40E+004	386.98	2.89E+005
m	23	675-	726	699.00	707.74	6.52	4.37E+004	430.32	4.59E+005
m	24	675-	726	718.10	724.36	6.53	1.92E+004	382.22	4.01E+005
M	25	736-	770	744.31	747.19	4.68	6.81E+003	339.10	2.10E+005
m	26	736-	770	762.85	763.32	4.69	2.10E+003	312.20	2.50E+005
M	27	803-	846	811.75	805.90	5.35	1.90E+004	346.97	2.01E+005
m	28	803-	846	841.25	831.58	5.38	7.64E+003	322.78	2.43E+005
	29	874-	891	883.22	868.13	4.97	4.47E+004	807.04	1.86E+005
M	30	983-	1016	990.57	961.58	4.74	6.09E+003	287.50	1.43E+005
m	31	983-	1016	1007.31	976.16	4.75	2.65E+003	270.42	1.93E+005
	32	1032-	1041	1035.25	1000.48	2.99	1.15E+003	442.33	8.60E+004
	33	1105-	1118	1109.08	1064.76	5.88	2.97E+003	550.35	1.09E+005
	34	1136-	1155	1146.20	1097.08	7.85	2.23E+004	761.95	1.59E+005
	35	1185-	1203	1195.00	1139.57	5.58	8.29E+003	690.70	1.39E+005
M	36	1260-	1286	1269.54	1204.46	6.96	1.82E+004	489.96	1.53E+005
m	37	1260-	1286	1276.60	1210.61	6.96	8.34E+003	511.80	1.87E+005
M	38	1363-	1406	1373.05	1294.58	5.30	1.75E+004	193.81	1.33E+005
m	39	1363-	1406	1379.26	1299.98	5.31	9.71E+003	174.29	1.71E+005
m	40	1363-	1406	1399.90	1317.96	5.32	3.11E+002	152.95	1.42E+005
M	41	1445-	1504	1454.28	1365.30	5.78	7.60E+003	244.62	1.18E+005
m	42	1445-	1504	1470.25	1379.21	5.79	6.02E+003	240.42	1.75E+005
m	43	1445-	1504	1494.61	1400.42	5.81	5.87E+003	243.58	1.66E+005
M	44	1558-	1630	1568.16	1464.45	6.22	1.15E+004	259.10	1.15E+005

Appendix C-2 Continued

	Peak No.	ROI start	ROI end	Peak centroid	Energy (keV)	FWHM (keV)	Net Peak Area	Net Area Uncert.	Continuum Counts
m	45	1558	1630	1578.11	1473.12	6.23	3.28E+003	241.31	1.69E+005
m	46	1558	1630	1598.52	1490.88	6.24	5.56E+003	234.02	1.77E+005
m	47	1558	1630	1621.25	1510.67	6.26	3.72E+003	231.71	1.68E+005
	48	1684	1699	1691.38	1571.73	2.63	8.49E+002	494.33	8.10E+004
	49	1712	1732	1722.45	1598.78	3.81	2.68E+003	620.40	1.05E+005
	50	1789	1805	1795.07	1662.00	5.47	2.61E+003	507.77	8.15E+004
	51	1830	1846	1837.45	1698.90	4.36	2.10E+003	506.96	8.13E+004
M	52	1920	1965	1930.90	1780.26	6.18	7.92E+003	227.75	9.97E+004
m	53	1920	1965	1954.91	1801.17	6.19	1.86E+003	207.46	1.48E+005
	54	2138	2156	2145.77	1967.33	8.63	2.45E+003	525.70	8.10E+004
	55	2220	2232	2224.71	2036.06	3.69	9.70E+002	372.48	5.23E+004
	56	2310	2325	2314.69	2114.40	2.79	1.44E+002	428.10	6.09E+004
	57	2431	2454	2442.73	2225.87	7.80	2.55E+004	622.85	9.05E+004
	58	2583	2596	2589.59	2353.74	1.65	7.23E+002	359.75	4.67E+004
	59	2699	2722	2710.66	2459.14	4.27	2.79E+003	555.24	7.63E+004
	60	2816	2831	2820.13	2554.45	1.30	6.10E+002	380.77	4.80E+004
	61	5226	5239	5231.36	4653.74	1.11	5.17E+002	223.03	1.78E+004
	62	5416	5429	5421.19	4819.01	2.26	1.99E+002	220.64	1.76E+004
	63	6598	6620	6613.49	5857.06	3.48	-9.66E+001	280.10	2.02E+004
	64	6775	6794	6783.50	6005.07	1.90	4.26E+002	241.51	1.65E+004
	65	6916	6937	6923.14	6126.64	1.26	4.36E+002	252.77	1.69E+004
	66	7004	7022	7014.66	6206.32	2.54	5.27E+002	225.96	1.49E+004
M	67	7162	7198	7175.86	6346.67	7.25	1.46E+003	117.83	1.93E+004
m	68	7162	7198	7187.06	6356.42	7.26	1.93E+003	139.24	2.65E+004
	69	7237	7251	7243.17	6405.27	1.79	3.69E+002	182.40	1.14E+004
	70	7753	7786	7769.95	6863.90	16.12	4.73E+003	305.70	1.69E+004
	71	7811	7842	7827.77	6914.24	6.35	1.79E+003	285.88	1.60E+004
	72	8066	8090	8076.51	7130.80	4.30	8.21E+002	209.01	1.04E+004
	73	8344	8378	8361.39	7378.82	13.05	2.75E+003	238.82	1.01E+004
	74	8397	8429	8414.05	7424.67	5.24	1.29E+003	215.69	8.82E+003
	75	8651	8675	8664.79	7642.97	2.66	4.51E+002	151.68	5.46E+003
	76	8982	9006	8990.69	7926.71	2.22	3.38E+002	122.90	3.57E+003
	77	9638	9658	9647.94	8498.93	2.73	1.14E+002	79.46	1.71E+003
	78	9857	9877	9867.80	8690.35	1.78	1.88E+001	67.75	1.26E+003
	79	12256	12271	12263.04	10775.71	1.15	1.79E+001	12.35	4.31E+001
	80	12735	12750	12742.64	11193.26	5.77	2.10E+001	9.66	2.40E+001

M = First peak in a multiplet region
m = Other peak in a multiplet region
F = Fitted singlet

Errors quoted at 1.000 sigma

APPENDIX D

EFFICIENCY DATA AND CALCULATIONS

^{152}Eu- Efficiency Calculations Calculations

E (keV)	Calculated Efficiency	Genie Data
244.69	2.20E-04	2.20E-04
344.27	1.56E-04	1.57E-04
411.11	1.31E-04	1.20E-04
443.98	1.22E-04	1.30E-04
778.89	8.06E-05	8.01E-05
867.32	7.58E-05	8.18E-05
964.01	7.13E-05	6.99E-05
1085.78	6.62E-05	6.87E-05
1112.02	6.52E-05	6.45E-05
1407.95	5.28E-05	5.27E-05

Chlorine Efficiency

E (keV)	Calculated Efficiency
517.07	1.07E-04
786.30	8.01E-05
788.43	8.00E-05
1131.25	6.44E-05
1162.74	6.31E-05
1164.87	6.30E-05
1601.07	4.43E-05*
1951.14	2.95E-05*
1959.35	2.92E-05*

Cadmium calculated efficiencies.

E (keV)	Calculated Efficiency
558.32	1.00E-04
651.19	9.00E-05
805.85	7.90E-05
1209.65	6.11E-05
1364.3	5.46E-05
1399.54	5.31E-05

* Estimated values based on Europium data, not accurate.

**N/A -Efficiency data cannot be extrapolated using derived using ^{152}Eu efficiency data.

APPENDIX E

PREDICTIVE CALCULATIONS FOR Cl, Cd and V

Appendix E-1. Theoretical Calculations of expected peak area counts of the most intense prompt gamma ray of Cadmium.

A	Isotope	Z	E(γ) Value	Sigma (b)	Fluence rate ($ncm^{-2}s^{-1}$)	Efficiency (s^{-1})	mNa/M 0.64g of Cd	Cps	Counts for 2000 secs Theoretical	Measured
113	114-Cd	48	558.32	1860	9.30E+05	1.00E-04	3.41E+21	5.92E+02	1.18E+06	2.35E+05
113	114-Cd	48	651.19	358	9.30E+05	9.00E-05	3.41E+21	1.02E+02	2.04E+05	4.71E+04
113	114-Cd	48	805.85	134	9.30E+05	7.90E-05	3.41E+21	3.36E+01	6.72E+04	1.94E+04
113	114-Cd	48	1209.65	122	9.30E+05	6.11E-05	3.41E+21	2.37E+01	4.73E+04	1.82E+04
113	114-Cd	48	1364.3	123	9.30E+05	5.46E-05	3.41E+21	2.13E+01	4.26E+04	7.63E+03
113	114-Cd	48	1399.54	97.7	9.30E+05	5.31E-05	3.41E+21	1.65E+01	3.29E+04	5.87E+03

Appendix E-2. Theoretical Calculations of expected peak area counts of the most intense prompt gamma-ray of Chlorine.

A	Isotope	Z	E(γ) Value	Sigma (b)	Fluence rate ($ncm^{-2}s^{-1}$)	Efficiency (s^{-1})	mNa/M 6.3748g of NaCl	Cps	Counts for 2000 secs Theoretical
35	36-Cl	17	517.073	7.58	9.30E+05	1.07E-04	6.47E+22	4.86E+01	9.72E+04
35	36-Cl	17	786.302	3.42	9.30E+05	8.01E-05	6.47E+22	1.65E+01	3.30E+04
35	36-Cl	17	788.428	5.42	9.30E+05	8.00E-05	6.47E+22	2.61E+01	5.22E+04
35	36-Cl	17	1131.25	0.626	9.30E+05	6.44E-05	6.47E+22	2.42E+00	4.85E+03
35	36-Cl	17	1162.739	0.76	9.30E+05	6.31E-05	6.47E+22	2.88E+00	5.77E+03
35	36-Cl	17	1164.865	8.91	9.30E+05	6.30E-05	6.47E+22	3.38E+01	6.75E+04
35	36-Cl	17	1601.072	1.21	9.30E+05	4.43E-05	6.47E+22	3.22E+00	6.45E+03
35	36-Cl	17	1951.14	6.33	9.30E+05	2.95E-05	6.47E+22	1.12E+01	2.25E+04
35	36-Cl	17	1959.346	4.1	9.30E+05	2.92E-05	6.47E+22	7.20E+00	1.44E+04

Appendix E-3. Theoretical Calculations of expected peak area counts of the most intense prompt gamma-ray of Vanadium

A	Isotope	Z	E(γ) Value	Sigma (b)	Fluence rate ($ncm^{-2}s^{-1}$)	Efficiency (s^{-1})	mNa/M 0.14g of V-51	Cps	Counts for 2000 secs Theoretical
51	52-V	23	125.082	1.61	9.30E+05	0.000326572	1.65E+21	8.07E-01	1.61E+03
51	52-V	23	147.846	0.253	9.30E+05	0.000314717	1.65E+21	1.22E-01	2.44E+02
51	52-V	23	419.475	0.249	9.30E+05	0.000128241	1.65E+21	4.90E-02	9.80E+01
51	52-V	23	436.627	0.397	9.30E+05	0.000123534	1.65E+21	7.53E-02	1.51E+02
51	52-V	23	645.703	0.769	9.30E+05	9.04807E-05	1.65E+21	1.07E-01	2.14E+02
51	52-V	23	823.184	0.32	9.30E+05	7.80737E-05	1.65E+21	3.83E-02	7.67E+01
51	52-V	23	845.948	0.252	9.30E+05	7.68775E-05	1.65E+21	2.97E-02	5.95E+01
51	**52-V**	**23**	**1434.10**	**4.81**	**9.30E+05**	**5.16280E-05**	1.65E+21	**3.81E-01**	**7.62E+02**
51	52-V	23	1558.843	0.323	9.30E+05	4.61622E-05	1.65E+21	2.29E-02	4.58E+01
51	52-V	23	5210.143	0.244	9.30E+05	4.61622E-05	1.65E+21	1.73E-02	3.46E+01
51	52-V	23	5515.813	0.39	9.30E+05	4.61622E-05	1.65E+21	2.76E-02	5.53E+01
51	52-V	23	5752.064	0.366	9.30E+05	4.61622E-05	1.65E+21	2.59E-02	5.19E+01
51	52-V	23	6464.887	0.43	9.30E+05	4.61622E-05	1.65E+21	3.05E-02	6.09E+01
51	52-V	23	6517.282	0.78	9.30E+05	4.61622E-05	1.65E+21	5.53E-02	1.11E+02
51	52-V	23	6874.157	0.49	9.30E+05	4.61622E-05	1.65E+21	3.47E-02	6.94E+01
51	52-V	23	7162.898	0.59	9.30E+05	4.61622E-05	1.65E+21	4.18E-02	8.36E+01

Appendix E-4. Theoretical Calculations of expected peak area counts of the most intense prompt gamma-ray of Cadmium corrected for self shielding

E (keV)	Atomic density	Cross section	Cps	Counts for 2001.6 secs		Discrepancy %
				Theoretical	Measured	
558.32	4.6286E+22	1860	62.16	124410.16	235000.00	-47.10
651.19	4.6286E+22	358	10.72	21466.16	47100.00	-54.46
805.85	4.6286E+22	134	3.53	7057.07	19400.00	-63.65
1209.65	4.6286E+22	122	2.48	4971.61	18200.00	-72.71
1364.3	4.6286E+22	123	2.24	4479.06	7630.00	-41.34
1399.54	4.6286E+22	97.7	1.73	3459.03	5870.00	-41.12

APPENDIX F

QUALITY ASSURANCE DATA SHEET OF THE ORTEC HPGE DETECTOR

QUALITY ASSURANCE DATA SHEET

GEM Series HPGe (High-Purity Germanium) Coaxial Detector System

DR6559

Model and Serial Numbers

Detector Model No.	GEM-23185-P
Cryostat Configuration	POP TOP
Dewar Model	—
Preamplifier Model	137CP2-2
Preamplifier S/N	#3378
H. V. Filter Model	138
H. V. Filter S/N	#5040

Important Reference Data

Ship Date 3-25-94

Serial No. 29-TP10374A

When calling Customer Service, always reference this Detector Serial No.

IF TEMP 29-TP10374A
TN217 RET 76394323-000002 RT ID: K5
KT-21-01-2-M -0010-8-05-04 21007471
SKP:KSB0105506-00011 CUST:105506 NRM
Srv: 05/25 5:00pm EDT For: CJONES|3 CYNTHIA JONES
R NEXT

Cryogenic Information

Dewar Capacity — Static Holding Time — Detector Cool-Down Time 6 Hrs.

Dimensions

Crystal Diameter	54.6	mm
Crystal Length	49.5	mm
End Cap to Crystal	3	mm
Total Active Volume	—	cc

Absorbing Layers

Aluminum	1.27	mm
Magnesium	—	mm
Inactive Germanium	700	μm

High Voltage Bias

Recommended Operation Bias, POSITIVE 3000 V

Performance Specifications*

	Warranted	Measured	Amplifier Time Constant
Resolution (FWHM) at 1.33 MeV, ^{60}Co	2.05 keV	1.64 keV	6 us
Peak-to-Compton Ratio, ^{60}Co	47.7	56.4	6 us
Relative Efficiency at 1.33 MeV, ^{60}Co	17.8 %	21.4 %	6 us
Peak Shape (FWTM/FWHM), ^{60}Co	1.90	1.86	6 us
Peak Shape (FWFM/FWHM), ^{60}Co	2.65	2.46	6 us
Resolution (FWHM) at 122 kev, ^{57}Co	— eV	— eV	

Other Capsule SCA # 1081
Cryo —

Data Certified By Gallagan Date 3-25-94

*Measured at a nominal rate of 1000 counts/s unless otherwise specified.

VITA

The author, Otu Effiong Inyang was born in Uyo, Nigeria. He received his Bachelor of Science (Hons) degree in physics from The University of Calabar, Nigeria in 1995. Prior to enrolling at Texas A&M University, he had a career spanning six years in commercial banking operations. During that period, he received a Master of Business Administration degree from the University of Calabar in Nigeria. He enrolled in the Health Physics program at Texas A&M University in August 2005 and received his Master of Science in Nuclear Engineering degree in August 2008. Otu is married with two children and enjoys spending time with his family.

Mr. Inyang can be reached at the Environmental Health & Risk Management Department, University of Houston, Texas 77204-1005 or through his email address oinyang@uh.edu.